



July–September rainfall in the Greater Horn of Africa: the combined influence of the Mascarene and South Atlantic highs

Ellen Dyer¹ · Linda Hirons² · Meron Teferi Taye³

Received: 6 February 2021 / Accepted: 2 April 2022 / Published online: 28 April 2022
© The Author(s) 2022

Abstract

July–September rainfall is a key component of Ethiopia’s annual rainfall and is a source of rainfall variability throughout inland Greater Horn of Africa. In this study we investigate the relative influences of the Mascarene (MH) and South Atlantic (AH) highs on July–September rainfall in a covarying region of the Greater Horn of Africa using CHIRPS observed rainfall and the ERA5 reanalysis. We show that a mixed metric using the circulation at 850 hPa of these two subtropical anticyclones (AH-MH), is better correlated with rainfall than individual high circulations. Variations in remote circulation are translated by changes in Central African westerlies and Turkana Jet wind speeds. We apply the AH-MH mixed metric to the CMIP5 and CMIP6 ensembles and show that it is a good indicator of mean July–September rainfall across both ensembles. Biases in circulation are shown to be related to the Hadley circulation in CMIP5 atmosphere-only simulations, while causes of biases in CMIP6 are more varied. Coupled model biases are related to southern ocean warm biases in CMIP5 and western Indian Ocean warm biases in CMIP6. CMIP6 shows an improved relationship between rainfall and Turkana Jet winds and Central African westerlies across the ensemble.

Keywords Africa · Precipitation · Atmospheric circulation · Subtropical high · General circulation models

1 Introduction

The July–September (JAS) rainfall signal in Africa is dominated by Sahel rainfall extending east to what Nicholson 2014 has called the summer regime of Ethiopia and Sudan. This season is critical for Ethiopia accounting for 50–80% of annual rainfall (Philip et al. 2018). However, JAS rainfall can be an important source of variability and uncertainty in other parts of the Greater Horn of Africa (GHA) (Davies et al. 1985) as shown in the 2020 season with lakes and dams in Western Kenya being at critically high levels (REACH 2020; African-SWIFT 2020). Understanding variability in this season, and how well this is represented in global

climate models used for future projections will be critical to development planning in this region.

While the El Nino–Southern Oscillation (ENSO) is a big driver of JAS rainfall variability (Gleixner et al. 2017), the influences of the Atlantic and Indian Ocean basins are also important (Segele et al. 2015, 2009b; Zeleke et al. 2013; Degefu et al. 2017) beyond simply modulating the impact of ENSO events (Fischer et al. 2005). For instance, Atlantic sea surface temperatures (SSTs) have been shown to have significant correlations with Ethiopian rainfall when ENSO effects were removed (Segele et al. 2009a; Camberlin et al. 2001). Two dominant features in these basins are subtropical anticyclones: the Mascarene High (MH) located between 20° and 40° S in the Indian Ocean, and the South Atlantic high (AH) located between 10° and 30° S in the Atlantic Ocean.

The MH and AH interact with another important feature in the JAS season, the Indian Monsoon. The transition to JAS is characterised by a shift in rainfall to higher latitudes and characterised by the development of the Somali Jet over the coast of East Africa and a shift to southerly flow across the equator that transports moisture into the Indian monsoon (Riddle and Cook 2008). Indian Monsoon rainfall has been

✉ Ellen Dyer
ellen.dyer@ouce.ox.ac.uk

¹ School of Geography and the Environment, University of Oxford, Oxford, UK

² National Centre of Atmospheric Science (NCAS), University of Reading, Reading, UK

³ International Water Management Institute, Addis Ababa, Ethiopia

shown to be positively correlated with GHA and East African rainfall through the modulation of the zonal pressure gradient which influences low level circulation and through the Tropical Easterly Jet (Camberlin 1995, 1997; Vizy and Cook 2003). However, the influence of monsoon strength has varying impacts through the GHA, and accounting for local circulation changes as a response to larger regional variability is important (Vizy and Cook 2003). The MH has been shown to have an impact on the intensification of the Indian Monsoon through westward movement of the MH and intensification of the cross-equatorial flow and Somali Jet (Terray et al. 2003; Vidya et al. 2020). However, monsoons and other regions of large-scale ascent such as the Hadley circulation have also been shown to influence the strength of sub-tropical anticyclones (Rodwell and Hoskins 1996, 2001). An inter-hemispheric influence has been shown in several modelling studies, with the Indian Monsoon shown to have an influence on the AH (Lee et al. 2013; Richter et al. 2008).

The MH has previously been implicated in East African rainfall using different metrics in both the October–December (OND) and JAS seasons. For example, Ogwang et al. (2015) showed in OND the position of the MH and its orientation are important indicators of moisture flux into East Africa with wetter conditions associated with a weaker MH that is shifted to the east. Manatsa et al. (2014) also argued that the zonal displacement of the high, described by the longitudinal position of the eastern ridge influences rainfall. Hiron and Turner (2018) showed that the eastern ridge shifting to the east is associated with a positive Indian Ocean Dipole (IOD) and increased rainfall in East Africa. Sun (1999) also examined OND rainfall in East Africa arguing that a weaker MH was associated with a southward shift in the Intertropical Convergence Zone (ITCZ).

During JAS, and further north in Ethiopia, a strengthening of the MH has been associated with wetter conditions. Studies show variation in the MH region has a positive relationship with Ethiopian JAS rainfall (Degefu et al. 2017; Segele et al. 2009b, 2015; Korecha and Barnston 2007), suggesting that MH intensity modulates the cross equatorial flow and moisture flux into Ethiopia (Degefu et al. 2017; Korecha and Barnston 2007), and the strength of the Somali Jet (Segele et al. 2015; Korecha and Barnston 2007). However, Crossett and Metz (2017) and Vizy and Cook (2020) show that nearer to the surface cross equatorial flow variability can result in cold air surges along the East African coast that inhibit rainfall locally. Segele et al. (2009a) also argue that a weakened MH, associated with warmer southern Indian Ocean SSTs, leads to reduced Ethiopian summer rainfall. However, they also state that the influence of Atlantic Ocean SSTs are more pronounced than Indian Ocean SSTs.

A number of studies evaluate the influence of the Atlantic in JAS, implicating the intensification of both the MH and

AH, with many arguing that the AH can modulate westerlies flowing from the Gulf of Guinea to eastern Africa (Korecha and Barnston 2007; Zeleke et al. 2013; Viste and Sorteberg 2013). Creese and Washington (2018) analysed Coupled Model Intercomparison Project Phase 5 (CMIP5) general circulation models (GCMs) over the Congo Basin during September–November and showed that wetter models had a stronger MH and AH, but that AH circulation differences were larger. Sun (1999) showed the importance of the South Atlantic high as a moisture source, but also in shifting the ITCZ further east during the short rains in East Africa during the OND season.

Many of these studies focus on seasonal predictability using observations or model experiments. There is less work on understanding the representation of these circulation features in GCMs such as the CMIP ensembles (Creese and Washington 2018) and none focused on how their representation influences modelled GHA rainfall. We will examine these features in CMIP5, and CMIP6 using a process-based assessment (James et al. 2018) as understanding the physical basis of projections is important if they are to be used in resilience planning (Rowell 2019). We pay particular attention to Ethiopia but take a different approach, scaling up to a larger region rather than dividing the country into small regional domains. We also examine how more local circulation features modulate the remote influence of the MH and AH on Ethiopian and GHA rainfall. This study aims to answer two questions:

- What are the relative strengths of, and mechanisms for, the influence of the MH and AH on Ethiopian and GHA rainfall in JAS?
- How do the CMIP5 and CMIP6 ensembles represent these two anticyclones and do they capture the relationship between the MH, AH and GHA JAS rainfall?

Models and datasets used in the study are described in Sect. 2. A description of relevant methods and how we select a region of interest for JAS rainfall in Ethiopia and GHA follows in Sect. 3. A mixed metric identified with rainfall and circulation composites is presented in Sect. 4. An evaluation of AH and MH in CMIP5 and CMIP6 are shown in Sect. 5. Finally, a discussion of these results and conclusions are presented in Sect. 6.

2 Datasets

We use the CHIRPS rainfall dataset on a monthly timestep for this study. The baseline period we use is 1981–2018 (38 years). We use CHIRPS because it incorporates both satellite based infrared cold cloud duration observations, and rainfall observations from an extensive network of

gauges (Funk et al. 2015). This rainfall dataset has been shown to be effective, and better at the monthly timescale than other rainfall products in Ethiopia and East Africa and includes more local station data than other datasets in the region (Funk et al. 2015; Dinku et al. 2018). To show that our results are not entirely dependent on the rainfall dataset used we also include alternatives to Figs. 1b, 3 and 7 using the TAMSAT v3.1 dataset (Maidment et al. 2017; Tarnavsky et al. 2014; Maidment et al. 2014) in Supplementary Figure 1.

For atmospheric fields we use the European Centre for Medium-Range Weather Forecasts (ECMWF) ERA5 reanalysis for the same baseline period (Hersbach et al. 2019). This reanalysis is an improvement on the ERA-Interim reanalysis, and was also selected because of its improved horizontal resolution at 31 km compared to 80 km of ERA-Interim and 50 km of MERRA5 (Hersbach et al. 2020). Sea surface temperatures (SSTs) are from the Met Office Hadley Centre's sea ice and SST data set (HadISST) (Rayner 2003). These SSTs are available at a monthly time step and $1^\circ \times 1^\circ$.

We use both coupled historical and AMIP simulations from the CMIP5 ensemble (Taylor et al. 2012). Our CMIP5 subset is limited to models run in both configurations and the r1i1p1 ensemble member, with the lowest forcing number used for each model. In the CMIP6 ensemble (Eyring et al. 2016) there are less AMIP/coupled historical pairs but we include a similar number of simulations from the same model families as CMIP5. Again, the r1i1p1 ensemble member with the lowest forcing number is used for each model in CMIP6. For both ensembles we select the common period of 1981–2005.

3 Regional rainfall and methods

3.1 JAS rainfall in Ethiopia and the Greater Horn of Africa

When examining Ethiopian climate most studies disaggregate Ethiopia into a number of smaller regions which are homogeneous by some metric. Nicholson (2014) divides Ethiopia into two, a summer and equatorial regime, while Degefu et al. (2017) expands this to three regions. In examining teleconnections to sea surface temperatures Diro et al. (2011) divides Ethiopia into six regions, whereas Riddle and Cook (2008) divided Ethiopia up into 4 separate regions based on CRU precipitation climatology. Viste et al. (2013) use 14 homogeneous rainfall zones to examine drought, while the National Meteorological Agency of Ethiopia divide Ethiopia into 8 homogeneous regions (Korecha and Sorteberg 2013). It is safe to say that examining Ethiopia's rainfall is made more complicated due to its heterogeneity.

We take the approach of expanding the regional analysis by examining regions that covary using the CHIRPS rainfall dataset. We divide Ethiopia into two regions, similar to those of Nicholson (2014), and focus on the northwestern portion of Ethiopia which has a broadly unimodal rainfall climatology with the highest rain rates in JAS (insert of Fig. 1a). We then calculate the spearman correlation, masked where the two-sided p-value is < 0.1 (Fig 1a) Northwest Ethiopian JAS rainfall is correlated with Sahel rainfall, but it is also strongly correlated with inland East African rainfall. Further masking this map by imposing a minimum correlation value of 0.5, the correlation with this East African region becomes clearer and forms the basis for masking a GHA JAS region. Our region

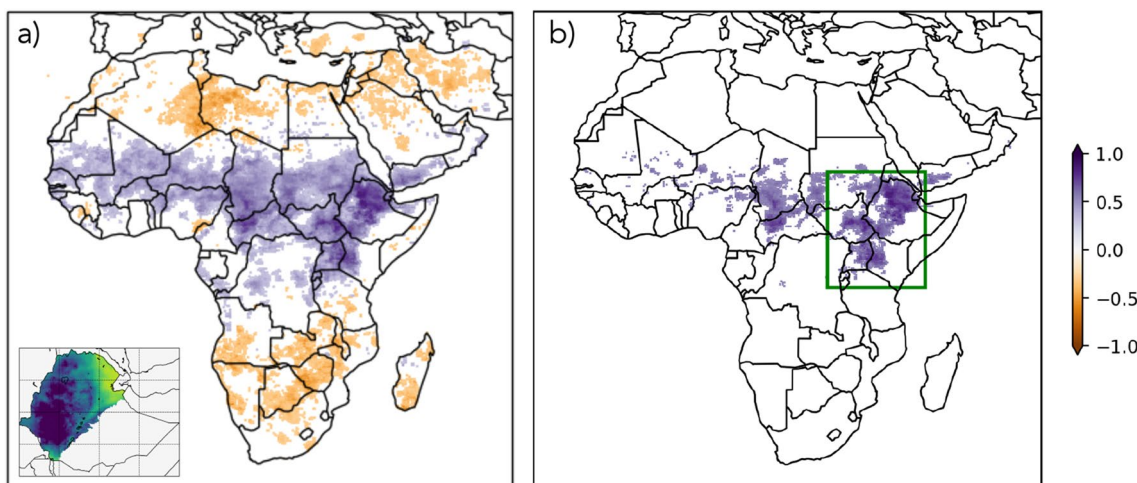


Fig. 1 Correlation between JAS northwest Ethiopia rainfall and African JAS rainfall. Masked for $p < 0.1$ in (a) and for spearman correlation > 0.5 in (b), using monthly CHIRPS rainfall from 1981 to 2018.

The GHA masked JAS rainfall region uses the highlighted grid points within the green box ($4^\circ S$ – $16^\circ N$, 27° – $44^\circ E$) in (b)

ends up being similar to Camberlin (1997) who used mean rainfall to decide on their region, then dividing it into northern and southern aggregate regions and Williams et al. (2012) who then divided their region using Bombay and Sudan-Mediterranean gradient sea level pressure. Although some of the masked area will not have JAS as the main rainy season, there is still importance in this season. For example, the Turkwel river basin (REACH 2020) in northwestern Kenya has a trimodal rather than bimodal rainfall climatology, unlike other parts of Kenya, with the JAS season having higher rain rates than the OND season. As we are interested in using the inter-annual variation in the JAS season to identify important relationships this region suits the purpose of this study.

The interior GHA region we use for the remainder of this study is shown as the masked region within the green boundary in Fig. 1b and will be referred to as ‘GHA masked’ throughout the study.

3.2 Methods

The eastern ridge longitude of the MH was calculated using the methods outlined in Manatsa et al. (2014) and Hiron and Turner (2018). First the location of maximum geopotential height in the longitudinally averaged region 0° – 45° S and 15° – 120° E is found. The longitude where the 1540 m geopotential height contour intersects the latitudinal maximum is considered to be the eastern ridge longitude.

AH and MH circulation was explicitly calculated using a similar approach to Randel and Park (2006), who used this to measure the strength of the anticyclonic flow of the Indian monsoon in the upper troposphere along a contour of constant geopotential height. This method has been similarly applied by He et al. (2017) using characteristic contours for vorticity to measure future changes in subtropical anticyclones. Here we use the 1540 m geopotential height contour in the lower troposphere at 850 hPa, consistent with other metrics for the MH. The AH region is (0° – 40° S, -60° – 15° E), the MH region is (10° – 45° S, 10° – 120° E). The definition of circulation is

$$C = \oint \mathbf{U} \cdot d\mathbf{l} = \oint (u dx + v dy) \quad (1)$$

However, for ease of calculation, we compute the area integrated relative vorticity within this contour, equivalent via Stokes’ theorem (Randel and Park 2006; Holton and Hakim 2012).

We also use 200 hPa velocity potential (χ) representing upper-tropospheric divergence to identify large-scale tropical circulations.

$$\nabla \cdot \mathbf{V} = -\nabla^2 \chi \quad (2)$$

\mathbf{V} is the horizontal wind vector at 200 hPa. We use the windspharm spherical harmonics library for this calculation

Dawson (2016). We also apply a decomposition to 200 hPa velocity potential detailed in Tanaka et al. (2004):

$$\chi(t, x, y) = [\chi(t, y)] + \chi^*(x, y) + \chi^{*'}(t, x, y) \quad (3)$$

The first term is a zonal mean representing the Hadley circulation, the second term is the time mean eddy component representing the Walker circulation, and the third term is the transient eddy component representing the monsoon circulation.

In this study we composite the most extreme 8 wet and dry JAS GHA masked rainfall seasons in CHIRPS. We also create composites of the 8 weakest and strongest JAS seasons of AH and MH circulation in ERA5. We calculate composite differences against the 38 year JAS baseline (composite average–baseline average) and significance with a method suitable for small samples described by Boschat et al. (2016) originally proposed by Terray et al. (2003). Here we applied it to spatial maps of composite differences in Sect. 4. We use a random distribution of 1000 composites and apply a critical threshold of 0.1. We use the same compositing approach for CMIP5 and CMIP6, however the wettest and driest 5 JAS seasons are used to create wet and dry composites from the shorter 25 year baseline. Correlations are calculated using the Spearman correlation coefficient (r) with an accompanying two-sided p-value or mask (usually $p < 0.1$).

The following regional definitions are used throughout the study. Cross equatorial flux is measured over 5° S– 5° N, 40° – 53° E at 850 hPa. The strength of the Somali Jet is measured as in Boos and Emanuel (2009) over 5° – 20° N, 50° – 70° E at 850 hPa. We create a Turkana jet (TJ) index by taking the average of 850 hPa wind speed in the Turkana channel region 1° – 8° N, 32° – 38° E. Finally, we create an index for the westerly flux originating from Central Africa (CAF) using wind speed in the region 4° – 12° N, 18° – 30° E similar to that defined in Taye et al. (2021).

4 Rainfall and circulation composites

Wet and dry GHA masked JAS composite differences (years shown in Table 1) of lower tropospheric winds and geopotential height (Fig. 2b, d) show anomalies in both the Indian and Atlantic Oceans. In the Indian Ocean there are increased (decreased) westerlies between 30° and 40° S in wet (dry) seasons. These wind changes overlay a decrease (increase) in geopotential height south of 30° S in wet (dry) seasons. These changes in southern Indian Ocean SSTs are consistent with geopotential height changes throughout the basin, especially in the Arabian Sea. There is also a change in winds along the coast of East Africa and into the Arabian Sea with increased southwesterly flow in wet seasons and a weakening of this flow in dry seasons resulting in

Table 1 Years used in wet and dry JAS season composites, and strong and weak composites for MH and AH circulation

Composite JAS seasons	Years
Dry masked GHA	1987 1984 2009 1997 2015 2002 1993 1986
Wet masked GHA	2001 2003 2011 1998 2017 2007 2012 1988
Weak AH	1984 1989 1981 1983 1985 1993 1996 2008
Strong AH	1998 2007 1991 2016 2017 2013 1995 2012
Weak MH	1996 1984 1981 1988 2011 1983 2013 2001
Strong MH	1982 1997 2018 2005 2006 1994 2004 2002

Where circulation composite years correspond to dry years they are underlined, and where they correspond to wet years there are shown in bold

weaker flow in the Turkana channel region during wet seasons and stronger flow in dry seasons. In the Atlantic basin wet (dry) seasons are associated with an increase (decrease) in geopotential height in the south Atlantic. These changes in geopotential height are accompanied by an increase in southerly cross equatorial flow, and increased (decreased) westerlies across the southern coast of West Africa in wet (dry) composites. Figure 2a and c highlight the 1540 m geopotential height contour which show the spatial extent of the MH being smaller in wet composite than it is in the dry composite while the opposite is true for the AH.

Given the previous connections found between the position and eastern extent of the MH with East African rainfall

(Hirons and Turner (2018); Manatsa et al. (2014); Ogwang et al. (2015)) we calculated the eastern ridge longitude (ER) of the MH in baseline, wet and dry composites. There is a consistent change in composite ER, with an eastward extension associated with less JAS GHA masked rainfall. This relationship is also true for the majority of CMIP5 models (see Supplementary Figure 2). A more eastern ER, associated with dryer conditions in JAS, is actually the opposite of the connection between an eastward shift and wetter conditions found for East African OND rains (Hirons and Turner (2018); Ogwang et al. (2015)). However, this more eastern ER would be an indication that the MH has not shifted to the west and intensified in a way that has been shown to positively influence the summer Indian Monsoon in JAS through low-level circulation and a modulation of the local Hadley circulation (Terray et al. 2003). This would be consistent with previous studies indicating that a more eastward MH is associated with a weaker Indian Monsoon and also lower rainfall in much of the GHA (Camberlin 1995, 1997; Vizy and Cook 2003). Although there is a consistent relationship between ER and composite rainfall, correlation of the long term GHA masked rainfall and ER is low at -0.12 ($p = 0.46$). This was also tested with northwest Ethiopian rainfall and this correlation was -0.06 ($p = 0.74$).

4.1 Two southern highs: the South Atlantic High and the Mascarene High

While the positions of the MH and AH are not well correlated with GHA masked rainfall, the strength of these systems do change in wet and dry composites. Because these systems have been associated with rainfall changes and a

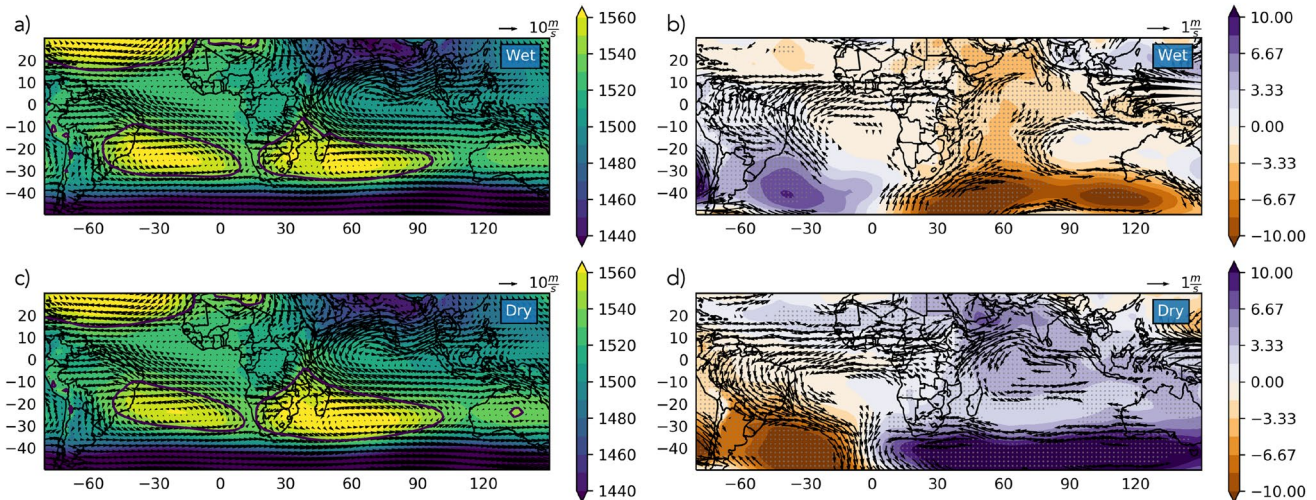


Fig. 2 850 hPa geopotential height (m), with a 1540 m geopotential height contour overlaid with 850 hPa winds (m/s), for **a** the wet composite JAS GHA masked rainfall, and **c** dry composite JAS GHA masked rainfall. Wet (**b**) and dry (**d**) composite differences (com-

posite-full baseline) are in the second column. Composite difference wind vectors are shown where either meridional or zonal wind differences are significant at a 0.1 threshold, and grey stippling indicates a geopotential height difference significant at a 0.1 critical threshold

change in moisture flows to GHA, we have calculated the circulation strength of these two anticyclones in an effort to measure this influence more directly (see Sect. 3.2). The spatial correlations of these two circulation strengths and African JAS rainfall are shown in Fig. 3. AH circulation is positively correlated with eastern Sahel and northern Ethiopian rainfall, while MH circulation is negatively correlated with GHA rainfall further south, including some areas in southern Ethiopia. This indicates that there might be value in using an index that combines the strength of these two highs. The correlation of GHA masked JAS rainfall and MH circulation is -0.30 ($p = 0.06$), while for AH the correlation is 0.36 ($p = 0.03$). However, the correlation of the difference between these two circulation strengths (AH-MH) is 0.47 ($p < 0.01$).

Composite means determined using strong and weak circulation strength for each high are shown in Fig. 4a–d highlighting the spatial extent and intensity of the highs, while the composite differences are shown in Fig. 4e–h. Years for composite JAS seasons are summarised in Table 1. There is some overlap between wet seasons and strong AH and weak MH, and dry seasons and weak AH and strong MH.

In strong MH composites there is expansion and intensification of the high. In the strong MH case there is increased inflow to eastern Africa due to an increase in cross equatorial flow in the eastern and central Indian Ocean which splits to weaken southerly flow in the western Indian Ocean (similar to Fig. 2d) but increase local westerly flow across India. In the weak MH composite the high is greatly reduced in extent and southeasterly flow is weakened with westerly anomalies extending to Central Africa. In the AH composite differences there is a change in westerly flow in the same

northern boundary of the Congo Basin which extends west to the Atlantic. This change is westerly in the strong AH composite, and weaker and easterly in the weak AH composite. The influence of a strong AH seems to have more impact than a weak AH.

The complementary effect of a weakened MH and strengthened AH (and vice versa) on GHA masked rainfall is shown in Fig. 5 with increased rainfall composite differences across the top row, and decreased rainfall composite differences across the bottom row. The wet GHA masked composite (Fig. 5a) shows the concurrent increase in rainfall across the eastern Sahel, Ethiopia, and the inland region of East Africa. The strong AH composite (Fig. 5b) shows a similar, although less intense increase while the weak MH (Fig. 5c) change has isolated inland East Africa increases, opposite in sign to the Sahel change, without a distinct increase in rainfall in northern Ethiopia. GHA masked dry composite rainfall differences (Fig. 5d) are opposite and similar in spatial extent to wet differences. The same can be said for the strong MH composite difference (Fig. 5f), which again isolates changes in the GHA from the Sahel. However, the weak AH composite rainfall difference (Fig. 5e) changes are mostly confined to decreases in the Sahel and northern Ethiopia. This asymmetric difference between the AH weak and strong composite rainfall patterns can be related back to the difference in strength of the change in 850 hPa westerlies in Fig. 4e and g and more local circulation changes (Sect. 4.2).

4.2 Local circulation pathways

Given the potential remote influence of the MH and AH on GHA rainfall we investigate how these highs might modulate

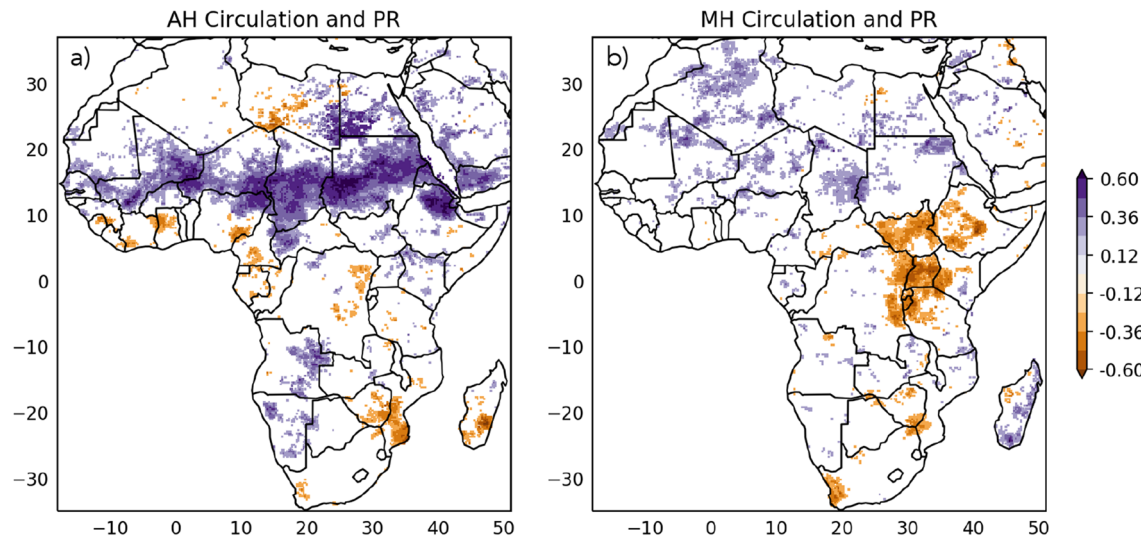


Fig. 3 Spearman correlations between **a** JAS AH circulation and rainfall in Africa, and **b** JAS MH circulation and rainfall in Africa. Correlations are masked for p-values above 0.1 using the baseline 1981–

2018 time series for CHIRPS rainfall and circulation calculated using 850 hPa winds from ERA5

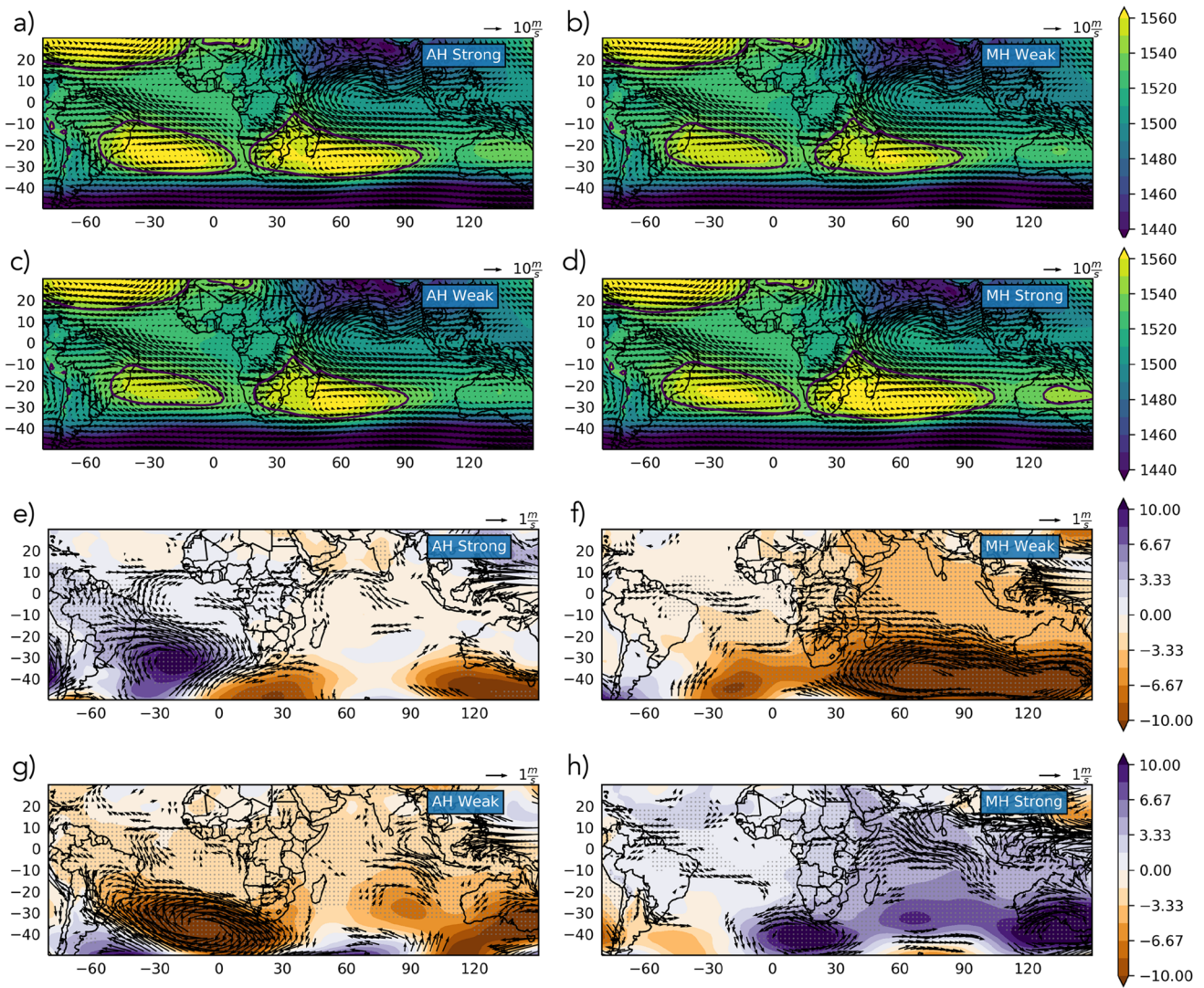


Fig. 4 Composites (**a–d**) and composite differences (**e–h**) for AH circulation (left) and MH circulation (right) JAS seasons. 850 hPa geopotential height (m) and horizontal wind composite means (m/s) with a 1540 m geopotential height contour are shown above composite dif-

ferences. Composite difference wind vectors are shown where either meridional or zonal wind differences are significant at a 0.1 threshold, and grey stippling indicates a geopotential height difference significant at a 0.1 critical threshold

local circulation features that in turn have a direct influence on rainfall. To do this we examine 850 hPa wind speed with mean JAS baseline wind speed shown in Fig. 6a. None of the composite changes involve flow reversal in the key features to be examined (not shown). A number of features stand out clearly in the GHA masked wet and dry composites (Fig. 6b,e) including winds in the Turkana channel (TJ), winds to the north of the Democratic Republic of Congo over Central African republic and South Sudan (CAF), winds off the coast in the Somali Jet region, and a cross equatorial flow region. In wetter conditions for all composites, TJ winds are weaker, and CAF winds are stronger. There is also agreement in wet composites on Somali Jet wind strength but AH and MH composite wind speed anomalies are weaker than

in the wet/dry composites. Composites with dry conditions show these same but opposite conditions except for the AH weak composite where the TJ winds do not strengthen and the CAF anomalies are shifted further north.

Strong AH changes do have many features that are similar to GHA masked wet composites. In particular, a strong AH is associated with a large CAF anomaly that is diverted by topography to the south of the Kenya highlands, to the Turkana channel, and around the Ethiopian highlands with increased northwesterly flow through the Red Sea into the north of Ethiopia (see Supplementary Figure 3).

Using wind speed averages in regions shown in Fig. 6b (see Sect. 3.2), we correlate wind speed with GHA masked rainfall, AH, and MH circulations. The winds most

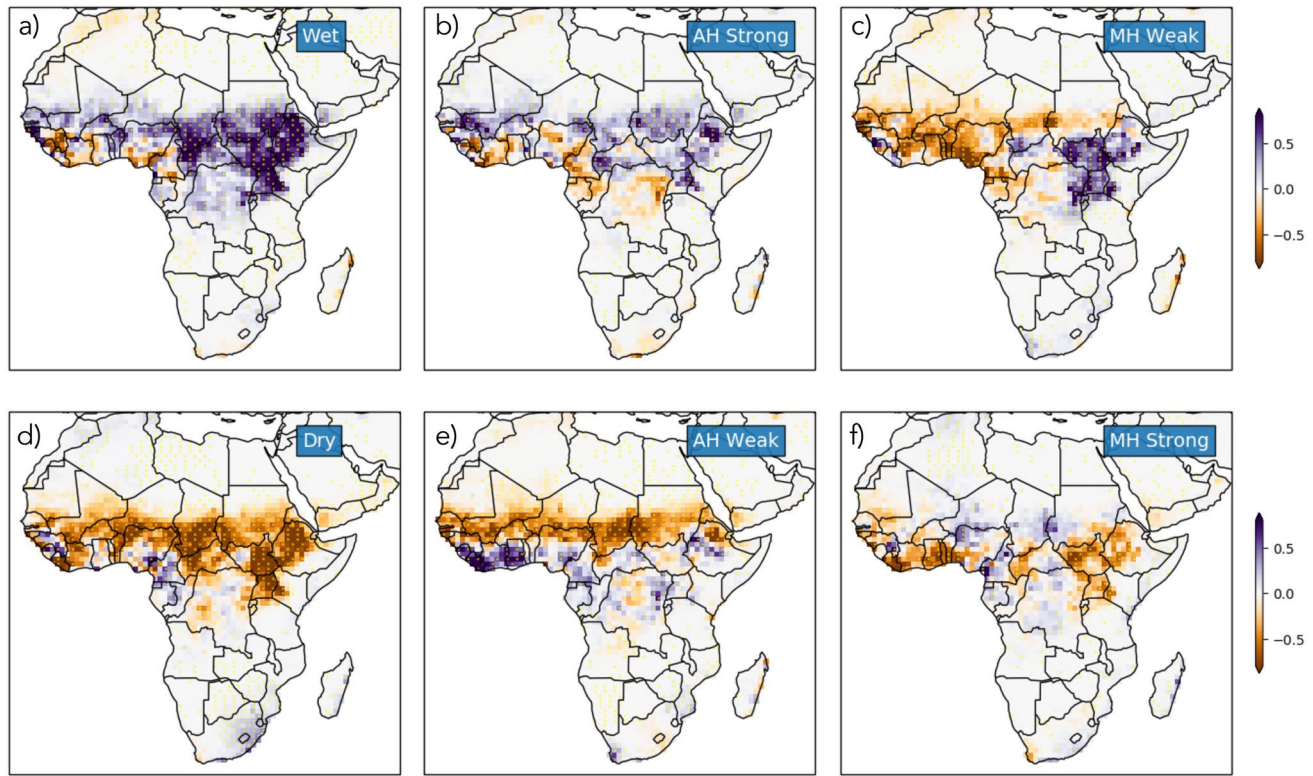


Fig. 5 Composite rainfall differences (mm/day) for **a** masked GHA wet, **d** masked GHA dry, **b** strong AH circulation, **e** weak AH circulation, **c** weak MH circulation, and **f** strong MH circulation JAS

seasons. Yellow stippling shows composite differences significant at a 0.1 critical threshold

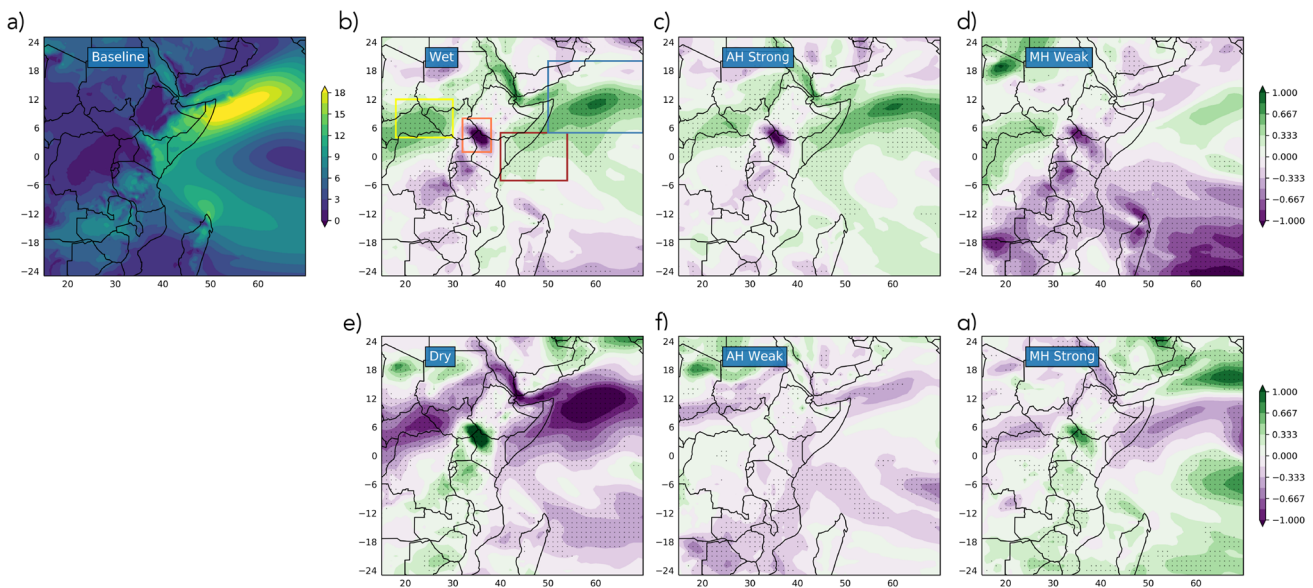


Fig. 6 **a** Wind speed (m/s) at 850 hPa shown for the baseline JAS 1981–2018 period. Composite differences for masked GHA rainfall wet and dry (**b**, **e**), strong and weak AH circulation (**c**, **f**), and weak and strong MH circulation (**d**, **g**) JAS seasons with stippling indicating significant differences at a 0.1 critical threshold. The red box is

for cross equatorial flow, measured over 5° S– 5° N, 40° – 53° E. The blue box is the Somali Jet region, measured over 5° – 20° N, 50° – 70° E. The orange box is the TJ index averaged over 1° – 8° N, 32° – 38° E. The yellow box is CAF winds over 4° – 12° N, 18° – 30° E

strongly correlated with rainfall are the TJ ($r = -0.74$, $p < 0.001$) and CAF ($r = 0.83$, $p < 0.001$) with the Somali Jet and cross equatorial flow having lower but significant correlations. In fact, a linear regression of CHIRPS GHA rainfall with CAF and TJ winds in ERA5 over the available period had a good fit ($R^2 = 0.75$) and reproduced this opposing relationship with CAF having a coefficient of 0.71 and TJ of -0.36 . The TJ winds are correlated with MH circulation ($r = 0.46$, $p < 0.01$), and Congo winds are better correlated with AH circulation ($r = 0.48$, $p < 0.01$). However, correlations between the wind speed in these two regions and AH-MH are stronger for the TJ ($r = -0.6$, $p < 0.001$) and CAF ($r = 0.54$, $p < 0.001$).

These local features that vary in both rainfall and circulation composites have previously been identified as controls on moisture pathways into Eastern Africa and Ethiopia (Taye et al. 2021; Viste and Sorteberg 2013). In agreement with our results the CAF was identified by Taye et al. (2021), Viste and Sorteberg (2013), and Williams et al. (2012) as being a moisture source for Ethiopian and GHA rainfall, with stronger moisture flux increasing rainfall in the highlands and the Awash basin regions. Moisture from the Indian Ocean is important for Ethiopian rainfall, but the TJ was not the most significant route for Indian Ocean moisture into Ethiopia (Viste and Sorteberg 2013). A strong TJ has also been implicated in moisture export from East Africa to the west, and strong divergence locally which causes decreased rainfall around the channel (Vizy and Cook 2019).

If we examine the correlations between local circulation and rainfall at shorter timescales (daily with a rolling mean of 5 days) the CAF and TJ still have the highest correlations, with the TJ having highest correlations leading rainfall by 2 days and CAF having highest correlations leading rainfall by 0–2 days. For correlations of circulation metrics with 850hPa winds with a 5 day rolling mean and various lead times the strongest correlations occur between local winds and AH-MH with winds lagging circulation by 2 days. However, the AH and MH timeseries have different characteristic power spectra (not shown) and we therefore applied a larger rolling mean window which showed improved correlations with similar lead times.

These results suggest that a mixed metric of relative AH and MH strength (AH-MH) is a good tool for understanding rainfall in the GHA masked region we identified in Sect. 3.1. The correlation map between the relative circulation strength metric (AH-MH) and African JAS rainfall is shown in Fig. 7 where the correlation is primarily with the GHA masked region, isolating the GHA and Ethiopia from the Sahel. The AH-MH mixed metric is particularly useful for Ethiopia where it relates to the western region that has a JAS rainy season and doesn't split north and south as the individual metrics did in Fig. 3.

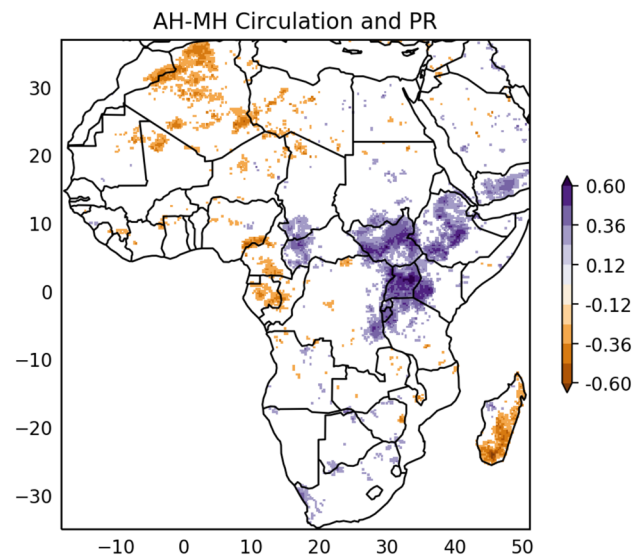


Fig. 7 Spearman correlation of the mixed circulation metric (AH-MH) and JAS rainfall in Africa. Correlations are masked for p -values above 0.1 and use the 1981–2018 time series for CHIRPS rainfall and circulation calculated using 850 hPa winds from ERA5

This metric relates to inland rainfall which may be less directly driven by coastal flows and local SSTs. In fact, GHA masked rainfall has very low correlations with JAS Indian Ocean SSTs above 20° S, the same being true for AH-MH circulation (see Supplementary Figure 4 for SST correlation maps). MH circulation is correlated with SSTs in the northwestern Indian Ocean, the south Atlantic, and the central and eastern Pacific. AH circulation is correlated with central Pacific SSTs and a SST dipole in the south Atlantic in JAS. However, both AH and MH JAS circulations are correlated (oppositely) with March–May (MAM) equatorial Atlantic SSTs. This is reflected in the GHA masked JAS rainfall correlations with MAM SSTs in agreement with Taye et al. (2021). JAS MH circulation is also correlated with MAM SSTs in the southeast Indian Ocean (also true for the JAS rainfall correlation with MAM SSTs). The influence of an anomalously cool southeast Indian Ocean and the corresponding persistence of MH amplification through the summer has been demonstrated by Terray et al. (2005). Therefore both elements of the mixed metric may be able to identify potential seasonal predictability indicators via their lagged correlations with SSTs. Beyond seasonal timescales, the mixed metric may be a useful way of understanding the influence of the Atlantic and Indian Ocean basins on GHA rainfall in a changing climate. MH circulation shows a small but statistically significant positive trend over the baseline period (Kendall's $\tau = 0.34$, $p < 0.01$) but AH, and AH-MH don't change significantly in strength. However, future warming will be differentially distributed across these basins and influence GHA rainfall remotely through the AH

and MH. Therefore understanding how models represent the AH and MH and their influence on rainfall in the historical period is a meaningful basis for understanding future change relationships.

5 The AH-MH in CMIP

The relationship between AH-MH circulation strength and mean GHA masked JAS rainfall in models is summarised in Fig. 8. In Fig. 8a (CMIP5) and b (CMIP6) models are ordered from driest to wettest, and as models get wetter the AH-MH difference tends to become smaller and eventually positive for some models. This relationship is quantified by positive correlations between rainfall and AH-MH across both CMIP5 ($r = 0.60$, $p < 0.01$) and CMIP6 ($r =$

0.62, $p < 0.01$). There are two additional results that can be summarised from these plots. First, most models vary in a similar way to ERA5 in that wet composites have higher AH-MH values and dry composites have lower AH-MH values. 35 out of 41 CMIP5 and 34 out of 39 in CMIP6 have a higher AH-MH in the wet composite mean. Second, for a majority of CMIP5 models, comparing the AMIP and Historical ensemble members, the wetter simulation has a higher AH-MH value (14 out of 22 pairs). This is also true for CMIP6 in all AMIP and Historical pairs but one, and is consistently true within model families even when there is not a direct AMIP-Historical pairing. This indicates that within model families the relationship is consistent but differences in baseline AH-MH need to be understood across the ensembles.

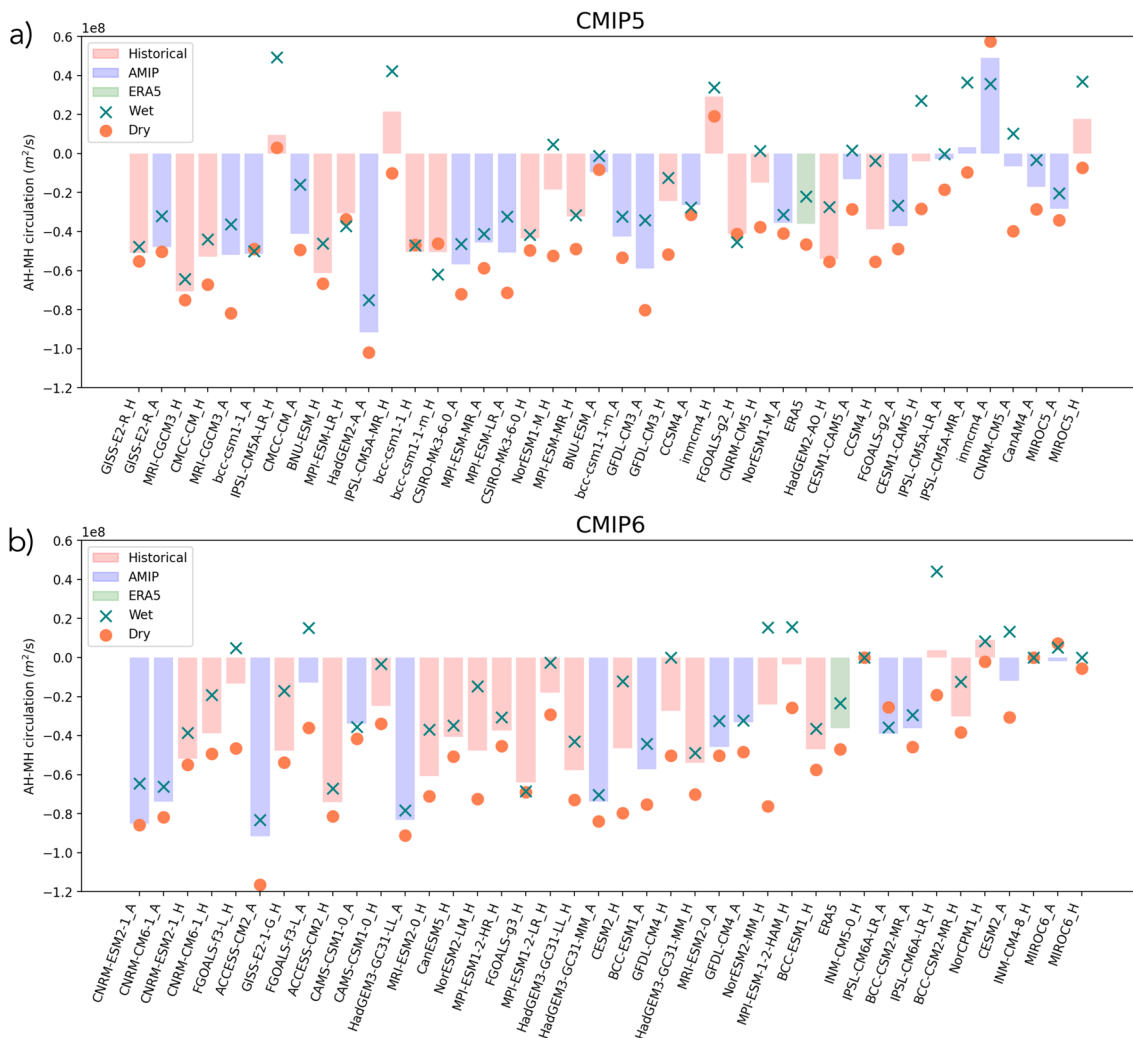


Fig. 8 The AH-MH circulation (m^2/s) in CMIP5 (a) and CMIP6 (b) models, ordered from driest to wettest along the x-axis. Bars represent baseline mean AH-MH circulation, where orange dots are the mean AH-MH circulation strength in dry GHA masked rainfall years

and green crosses are the same for wet years. Blue bars represent AMIP model simulations (A) and red bars represent coupled Historical simulations (H). The single green bar represents ERA5

There is a relationship between the AH-MH mixed-metric and JAS GHA rainfall in models across the larger ensemble and in model families however different models reproduce the strength of this relationship differently. There are also some consistent biases in model families in the two ensembles. To understand the inter-model and ensemble differences in performance we have examined the strength of both the AH and MH circulations and two local features identified using composites: the CAF and the TJ.

5.1 Southern highs in CMIP5 and CMIP6

5.1.1 CMIP5

There are a number of factors that can influence the strength of southern hemisphere highs including large-scale subsidence. In particular, Reboita et al. (2019) state the Hadley cell is the primary driver of AH during austral winter. As a proxy for the Hadley cell strength we used the decomposition of 200 hPa velocity potential suggested by Tanaka et al. (2004) (see Sect. 3.2) to distinguish between Hadley, Walker and monsoon overturning.

Figure 9 shows a subset CMIP5 AMIP (Fig. 9a) and Historical (Fig. 9b) simulations ordered based on the strength of JAS Hadley subsidence (20° – 40° S) over the southern oceans. We include a number of outliers as well as simulations that have AH and MH circulations close to ERA5 and have been shown to have skill for Ethiopian rainfall in the past (HadGEM2-A, MPI-ESM-MR, GFDL-CM3) (Dyer et al. 2020). The correlation of AH circulation with Hadley cell subsidence is high at -0.78 ($p < 0.01$), and -0.62 ($p < 0.01$) for MH circulation across AMIP simulations. The models with the weakest subsidence in AMIP (Fig. 10a) are inmcm4 and IPSL-CM5A-MR and both have very weak southern ocean highs. The AMIP simulation of MIROC5 has strong circulation in both the AH and MH and has the strongest subsidence (Fig. 10a). This changes in the Historical ensemble (Fig. 10b) with inmcm4 and IPSL-CM5A-MR still having weak Hadley overturning and weak highs but MIROC5 having much weaker AH and MH highs than its AMIP simulation. This is despite MIROC5 having the strongest subsidence in this ensemble.

Another aspect of the general behaviour in the two ensembles is that AMIP models tend to have stronger circulation in AH and MH (14/19 and 16/19 respectively for models that have both simulation types) in CMIP5. In CMIP5 this may be explained by coupled model SST biases. Figure 11a shows the ensemble mean of SST biases for CMIP5 which include a warm bias over the southern oceans (SO: 40° – 60° S, -180° – 180° E) that is particularly strong in the Indian Ocean (SIO: 40° – 60° S, 20° – 90° E). Biases in the SO are associated with weakened westerlies, although there is some disagreement on the cause of the biases. Wang et al.

(2014) argue that increased mixing of subsurface and surface waters due to biases in the Atlantic Meridional Overturning Circulation cause the warming, while Hyder et al. (2018) argue that warming is caused by net surface flux biases in the un-coupled models caused by shortwave biases due to errors in cloud representation.

We correlate the change in model circulation strength (coupled Historical - AMIP) with the SST biases (model-HadISST) shown in Fig. 11c. The full SO bias correlates well with AH circulation biases ($r = -0.81$, $p < 0.01$), and the SIO correlates well with MH circulation biases ($r = -0.79$, $p < 0.01$) across CMIP5 models. In this ensemble, MIROC5 is the most extreme outlier in the coupled Historical simulations but both inmcm4 and MIROC5 have the warmest southern ocean biases.

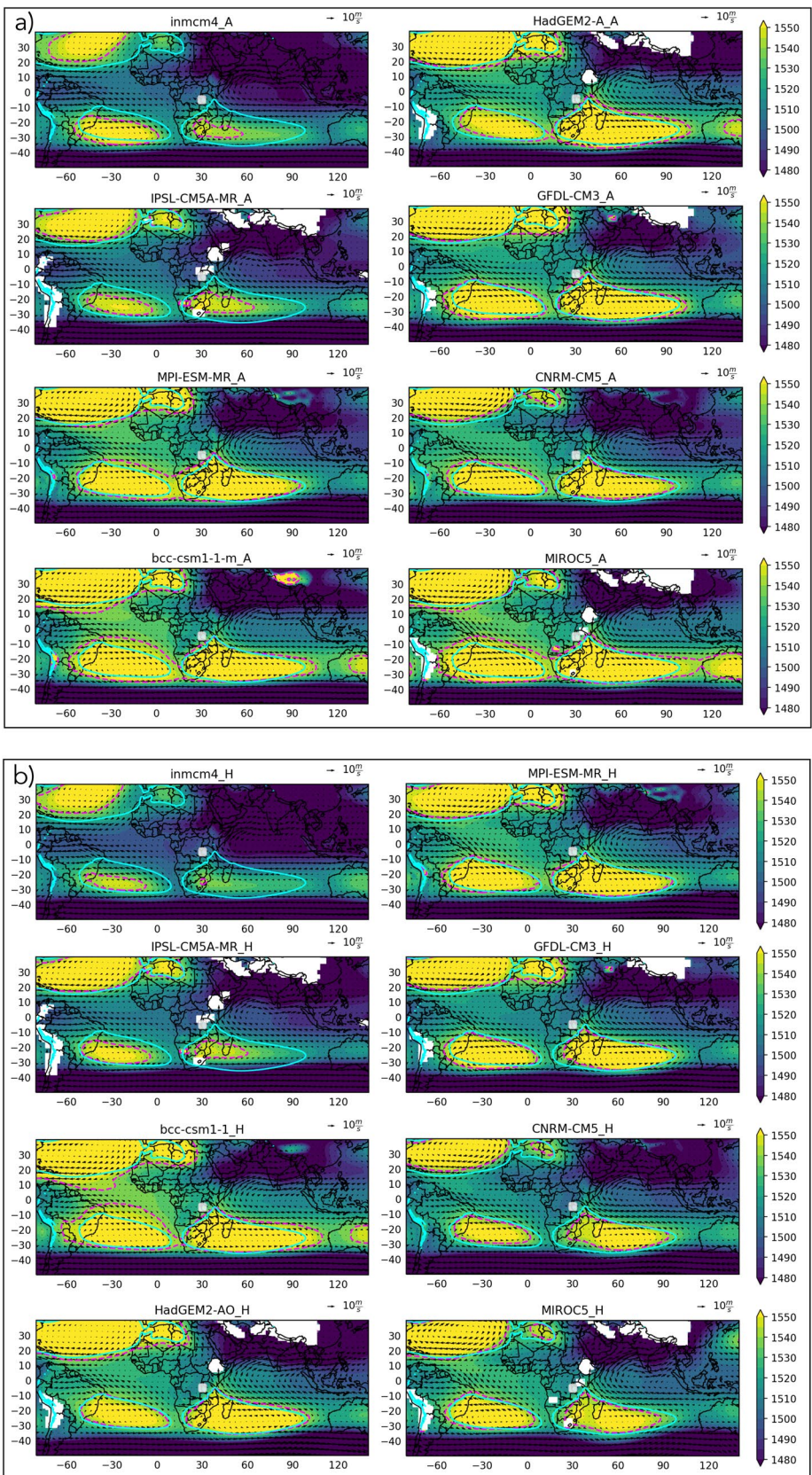
It is therefore possible to understand variation across CMIP5 AH and MH circulation using the strength of the descending branch of the Hadley circulation over the southern oceans in AMIP simulations with a stronger Hadley overturning associated with both stronger AH and MH circulations. In coupled simulations, SST biases in the southern oceans can help explain AH and MH circulation with a warm SO associated with a weak AH and a warm SIO associated with a weak MH.

5.1.2 CMIP6

CMIP6 is less easy to explain with this set of indices. Models in Fig. 12 are selected as in Fig. 9. In AMIP simulations the Hadley overturning circulation (Fig. 13a) is well correlated with AH strength if we exclude MIROC6 ($r = -0.67$, $p < 0.01$). Unlike in CMIP5, MIROC6 also has weak circulation in the AMIP simulation with the Historical circulation being even weaker. For CMIP6 we further examine all the components of the 200hPa velocity potential decomposition (Sect. 3.2). Richter et al. (2008) argued that there is a link between the AH and summer monsoons in the northern hemisphere and Lee et al. (2013) showed that such diabatic heating in the northern hemisphere produces subsidence in the tropical southern hemisphere and influences the strength of highs in the southern oceans. These studies suggest that there is an atmospheric link between the warm pool, Indian monsoon and circulation the tropical south Atlantic, indicating that there may be a remote influence on the AH strength. Therefore, we tested the strength of the Walker and monsoon overturning components against AMIP AH strength, with warm pool velocity potential being better correlated ($r = 0.74$, $p < 0.01$) than monsoon region velocity potential ($r = 0.48$, $p = 0.01$).

There are no clear correlations between MH strength and the components of the overturning circulation in across AMIP simulations. Some models have monsoon circulations that are very strong with increased downwelling

Fig. 9 850 hPa geopotential height (m) for a selection of **a** CMIP5 AMIP simulations and **b** CMIP5 Historical simulations. Contours in **(a)** and **(b)** are 1540 m geopotential height from each model (dashed pink) and the ERA5 reanalysis (solid green). Models are ordered based on their JAS zonally averaged 200 hPa velocity potential between 20° and 40° S



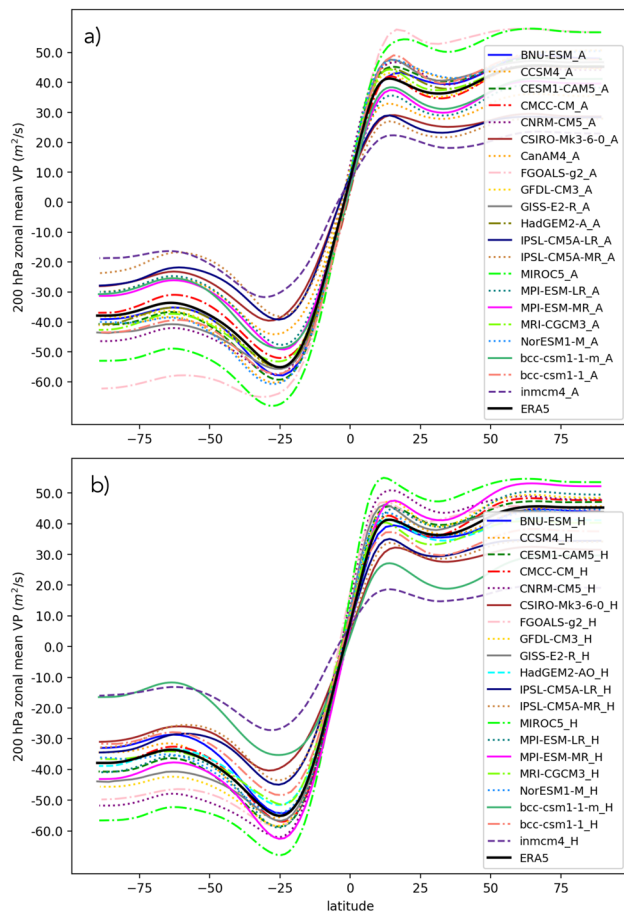


Fig. 10 JAS zonally averaged 200 hPa velocity potential between 20° and 40°S profiles for available **a** CMIP5 AMIP and for **b** CMIP5 Historical simulations

in the southwest Indian Ocean and a stronger MH (HadGEM-GC31-LL (Fig. 14c). Some models also have strengthened but shifted Walker circulations with down-welling over Africa, decreasing AH strength but increasing African subsidence, potentially creating poor conditions for GHA masked rainfall in multiple ways (HadGEM3-GC31-LL, CNRM-ESM2-1 (Fig. 14d)). In many cases, it is a combination of circulation components that can explain circulation strength. For example, to explain why CESM2 has the strongest AH in the ensemble but MH close to ERA5 (see Supplementary Figure 5 for individual AH and MH model circulation strength), we must consider its relatively strong Hadley component (Fig. 13a), westward shifted monsoon component (Fig. 14c), and relatively strong Walker overturning component (Fig. 14d). One model we cannot explain as easily is MIROC6, which remains an outlier.

In general, overturning circulations weaken in coupled models compared to their AMIP counterparts (Fig. 14c, d) and this is reflected in the strength of the highs (AMIP: Fig. 12a), coupled: Fig. 12b). Compared to CMIP5 a

smaller ratio of AMIP vs coupled model pairs has stronger AH circulation (8/14) while a larger ratio has stronger MH circulation (12/14) in CMIP6. However, there is no strong inter-model correlation for any of the circulation components. Similarly, SST biases also can't explain AH and MH biases as clearly as they did in CMIP5. Most models have a warm SO bias of over one degree, and there is no significant relationship between MH circulation strength and SIO bias (we used absolute MH as many Historical simulations that do not have AMIP counterparts).

A potentially important region of SST bias in CMIP6 is in the western Indian Ocean off the coast of East Africa (WIO: -5° – 15° N, 45° – 65° E) (Fig. 11b). This bias is warmer and more widespread in CMIP6 and alters the meridional SST gradient in the western Indian Ocean. It is also a region shown to correlate with MH circulation using ERA5 and HadISST (see Supplementary Figure 4c). Comparing MH circulation and western Indian Ocean SST bias (Fig. 11d) there appear to be two model groups: one with a nearly linear relationship between MH strength and IO bias ($r = 0.86$, $p < 0.01$), and another group that have weaker MH circulation than the first group.

In this second outlier group, MIROC and the INM-MC models are familiar outliers with strong SIO biases. We can understand other models using circulation biases, but their behaviour is less easy to attribute to SST biases. For instance, GISS-E2-1-G has weak Walker and monsoon overturning but also a basin-wide warm bias in the Indian Ocean and a dipole bias in the south Atlantic (not shown) which is the opposite of the observed correlation pattern between AH and JAS SSTs (see Supplementary Figure 4d) that might have a bigger local effect on AH circulation. We also looked into a possible relationship between southeast tropical Atlantic (0° – 10° E, 20° S–0) biases and circulation biases. There was no clear relationship between these known SST biases for either AH or MH strength in both CMIP5 and CMIP6. This is slightly surprising, however there are a number of possible causes for these biases in atmospheric model components (Exarchou et al. (2018); Richter and Tokinaga (2020)), including biases in the AH representation (Cabos et al. 2017).

In summary, some CMIP6 models have unrealistically weak MH and AH circulation, including the IPSL-CM6A-LR, MIROC6, GISS-E2-1-G, INM-CM4-8, and INM-CM5-0 models. The strength of AMIP AH circulation is positively influenced by stronger Hadley and Walker circulations, while explaining MH circulation required multiple circulation components for individual models. Similarly, coupled model behaviour is harder to generalise in CMIP6 than CMIP5. Biases in northwest Indian Ocean SSTs are potentially related to model MH circulation, however biases in the southern and Atlantic Oceans must also be considered.

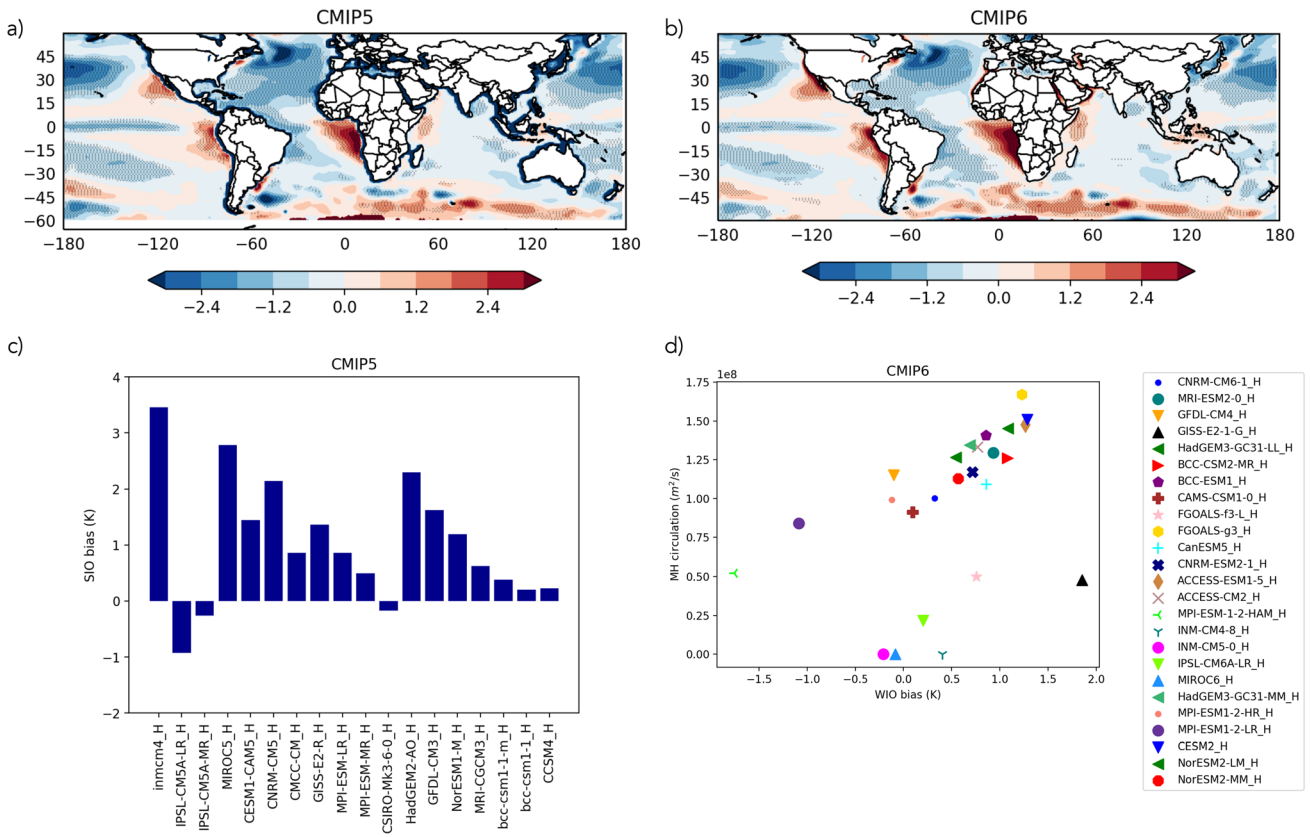


Fig. 11 Ensemble SST bias (K) averages for **a** CMIP5 Historical simulations and **b** CMIP6 Historical simulations. Stippling indicates 80% of available models agree on the sign of the bias. Biases are calculated relative to the HadISST sea surface temperature dataset.

5.2 Congo Basin flux and Turkana Jet in CMIP5 and CMIP6

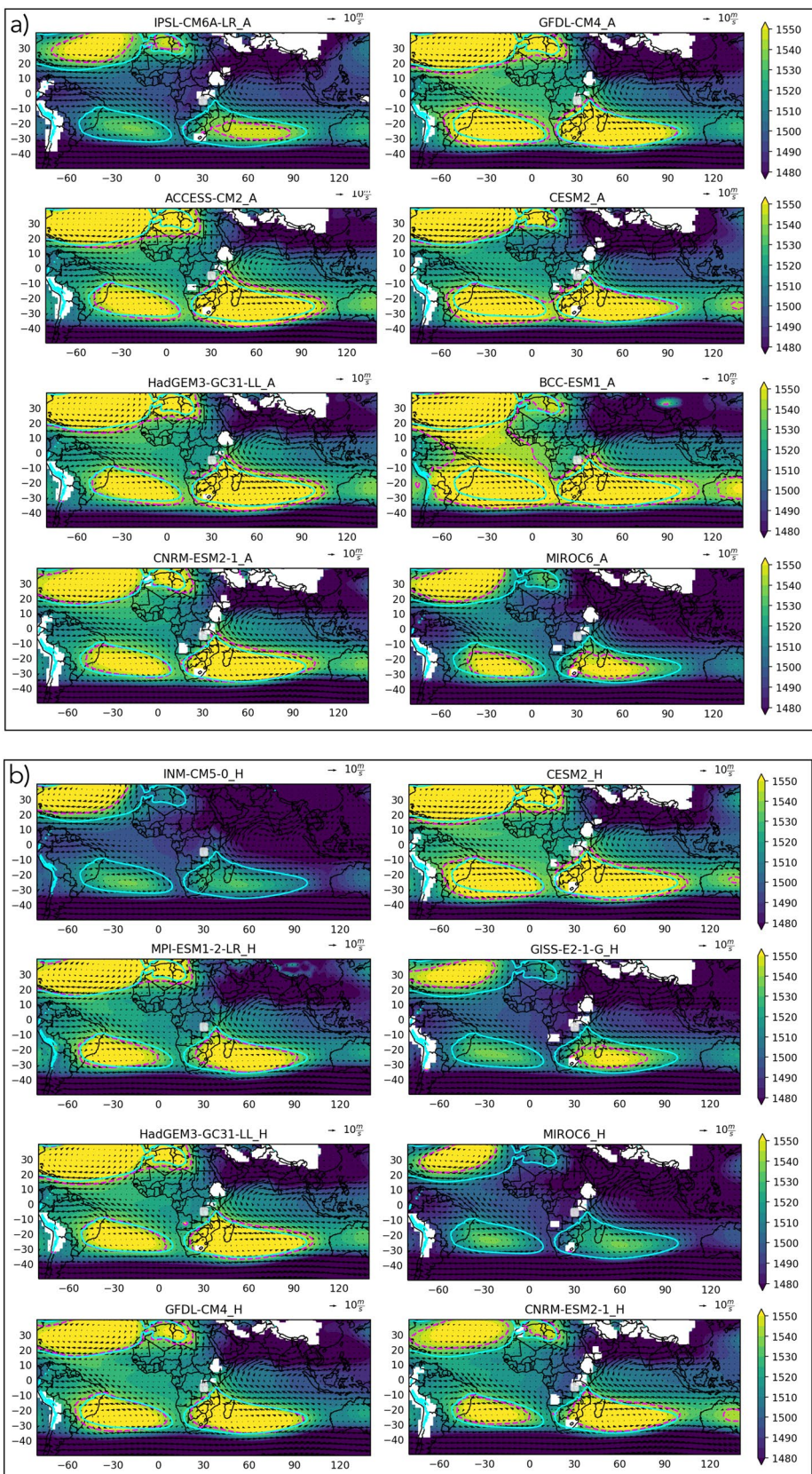
CAF, and TJ (see Sect. 3.2) wind speed across CMIP5, and CMIP6 are arranged in order of driest to wettest modelled GHA masked JAS rainfall in Fig. 15a and b, respectively. The majority of CMIP5 models have stronger CAF wind speeds than ERA5, with the driest five models having lower values, and the wettest models having much higher wind speeds. There is a significant correlation between mean model GHA masked rain rate and CAF flux ($r = 0.52$, $p < 0.001$), however there is a lot of variability within the ensemble. Conversely, there is no significant relationship between TJ flux and rainfall and a great deal of variability in CMIP5 with a range between 1 and 7 m/s. The driest models tend to have TJ flux values that are higher than CAF flux, and the wettest models tend to have CAF fluxes that are stronger than TJ fluxes. These results may reflect basic modelling issues in East Africa. The TJ flux metric does not evaluate whether wind in this region is part of a coherent jet, and many models in CMIP5 fail to adequately capture the Turkana channel due, in part, to coarse resolution.

c Model biases in the SIO region (40° – 60° S, 20° – 90° E) in CMIP5 ordered from weakest to strongest model MH circulation. **d** MH circulation vs western Indian Ocean SST biases (-5° – 15° N, 45° – 65° E) in CMIP6 historical simulations

In CMIP6 (Fig. 15b) these relationships become more consistent with a stronger positive correlation between mean model CAF flux and GHA masked rain rate ($r = 0.63$, $p < 0.001$) and a significant negative correlation between TJ flux and rain rate ($r = -0.53$, $p < 0.001$). There is less inter-model variability in CAF flux, and less models overestimating this wind speed than in CMIP5. There continues to be overestimation of the TJ flux in many models. It is an improvement that when there is an overestimation of one of these features, it is reflected in the GHA masked rain rate in CMIP6. Indeed, the strongly negative AH-MH circulation values and dry masked GHA rain rates in the CMIP6 CNRM models would seem to be translated via a strong TJ flux and relatively weak CAF flux. At the opposite end of the ensemble MIROC6 models have two of the weakest TJ flux values and relatively high CAF flux values.

Additionally, we performed a linear regression with CAF and TJ wind against GHA rainfall in JAS for CMIP5 and CMIP6 (see Supplementary Figure 6) in the same way as ERA5 in Sect. 4.2. 73% of models in CMIP5 and 79% in CMIP6 have a fit $R^2 > 0.5$ suggesting that beyond mean biases these local drivers are associated with inter-annual

Fig. 12 850 hPa geopotential height (m) for a selection of **a** CMIP6 AMIP simulations and **b** CMIP6 Historical simulations. Contours in **(a)** and **(b)** are 1540 m geopotential height from each model (dashed pink) and the ERA5 reanalysis (solid green). Models are ordered based on their JAS zonally averaged 200 hPa velocity potential between 20° and 40° S



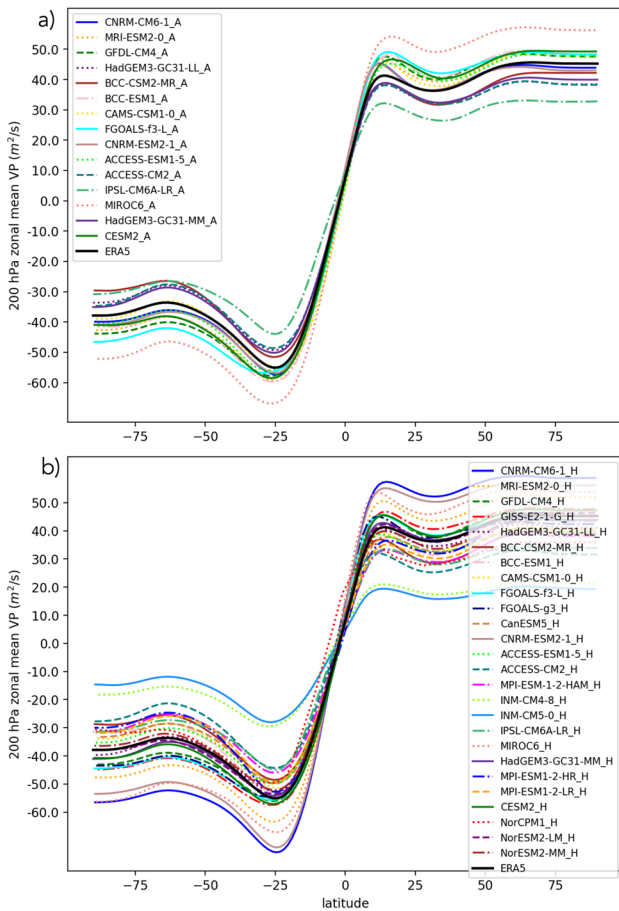


Fig. 13 JAS zonally averaged 200 hPa velocity potential between 20° and 40°S profiles for available **a** CMIP6 AMIP and for **b** CMIP6 Historical simulations

rainfall variability. This exercise also highlighted an improvement from CMIP5 to CMIP6, with models reproducing much more constrained CAF coefficients with no negative CAF coefficients in CMIP6. However, there continue to be models with positive TJ coefficients in CMIP6. These local circulation metrics indicate that some model GHA precipitation may be overly sensitive to particular local circulation pathways. This analysis suggests that the AH-MH mixed metric is related to rainfall by these local features in models and these local features would also be useful companion diagnostics of model performance, especially in the newer generation of CMIP6 models.

6 Discussion and conclusions

In this study we have developed a new mixed metric based on the relative circulation strength of the AH and MH. We investigated its influence on JAS rainfall using CHIRPS rainfall and the ERA5 reanalysis, identifying a region similar

to the GHA masked region we identified using correlations with Ethiopian JAS rainfall. We have also demonstrated its utility in understanding GHA rainfall in both the CMIP5 and CMIP6 ensembles. We draw the following conclusions about this metric and its connection to JAS GHA masked rainfall variability:

1. The AH-MH circulation mixed metric is better correlated with GHA masked rainfall than AH or MH circulation in isolation. A positive change in this metric is associated with increased rainfall.
2. AH circulation change drives changes in CAF westerlies across the north of the Congo Basin which are connected to TJ flow and flow around the Red Sea into northern Ethiopia. Stronger AH circulation is associated with increased rainfall.
3. MH circulation drives changes in TJ strength and outflow across the north of the Congo Basin and easterlies in Tanzania. Stronger MH circulation is associated with decreased rainfall.

Our finding that a relatively strong AH causes an increase in GHA rainfall is consistent with its influence on other areas of Africa, shown in different seasons in previous studies (Creese and Washington 2018; Korecha and Barnston 2007; Sun 1999; Zeleke et al. 2013; Viste and Sorteberg 2013). Conversely, where previous studies have found that MH intensification is associated with increased JAS rainfall (Korecha and Barnston 2007; Segele et al. 2015, 2009a, b) we have found the inverse. However, unlike these studies, our metric is one of circulation strength rather than pressure or geopotential height, and the region of interest is not along the coast or isolated to Ethiopia, capturing the influence of different local drivers such as the TJ. The differentiation between the inland and coast JAS climate in Kenya has previously been associated with the strength of westerlies in the mid- to lower-troposphere (Camberlin 1996; Davies et al. 1985) and is in broad agreement with the results we have shown for the influence of the CAF and TJ winds on regional climate. However, understanding how different MH metrics based on sea level pressure, geopotential height, location and circulation capture the MH and its various influences on African and Indian Ocean climate would be useful to better understand the variability of the MH and its influence as a semi-permanent feature changes throughout the year.

The MH may become an important driver of regional climate as ENSO's influence on the Indian summer monsoon since the 1970s weakened and, based on regional sea level pressure, the MH has intensified (Febe et al. 2019). Looking beyond the JAS season, these circulation systems might add useful information to forecasts beyond what is given by ENSO as MAM SSTs and JAS circulation have significant correlations similar to Taye et al. (2021), and MH has

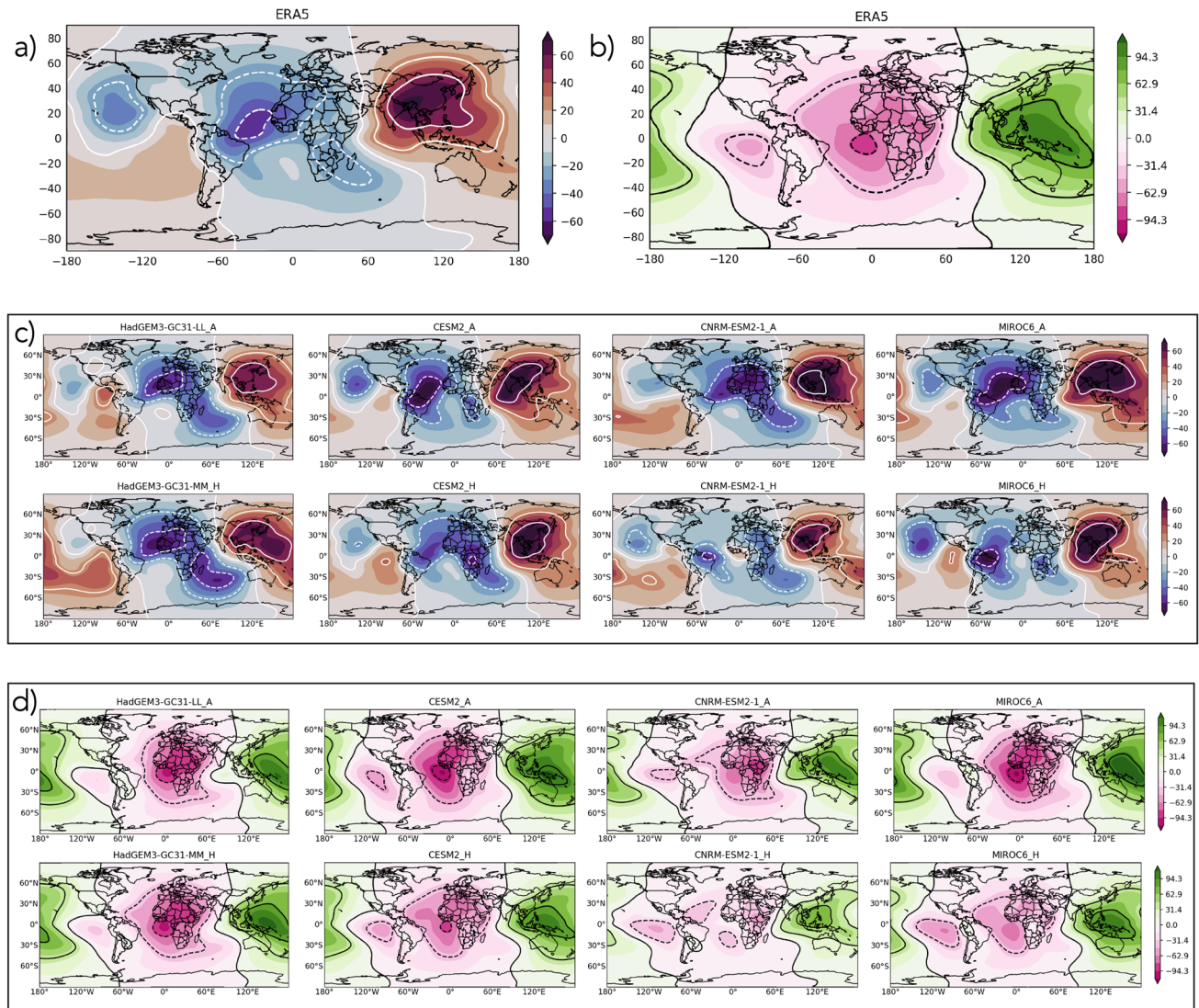


Fig. 14 Monsoon (a) and Walker (b) components of 200 hPa velocity potential (m^2/s) for ERA5 with the monsoon components of AMIP and Historical simulations from a selection of CMIP6 models in (c)

and Walker components of AMIP and Historical simulations from a selection of CMIP6 models in (d)

a significant negative correlation with the southeast Indian Ocean. Terray et al. (2005) have argued that SST anomalies in the southeast Indian Ocean during February–March can cause shifts in the MH. Through positive feedbacks these anomalies can persist through to the JAS season and influence the IOD and ENSO. However, to better understand these chains of impact it would be valuable to get a better understanding of the variability of both the MH and AH and feedbacks with other features like the Indian Monsoon on shorter timescales in JAS.

We also examined the relationship between AH–MH circulation strength and GHA masked rainfall in both the CMIP5 and CMIP6 ensembles. In doing so we demonstrated possible drivers of biases in AH and MH circulations in

AMIP and coupled Historical simulations. We also related this metric to the more local drivers of rainfall, the TJ and CAF winds. Based on this analysis we draw the following conclusions about the behaviour of the two ensembles:

1. Models in the CMIP5 and CMIP6 ensembles both have positively correlated mean GHA masked rainfall and AH–MH circulation.
2. In both ensembles wetter models within a model family tend to have more positive AH–MH. AH–MH becomes more positive in wet GHA masked composites and more negative in dry composites.
3. In CMIP5, biases in AH and MH are explained by the strength of large-scale descent in the southern hemi-

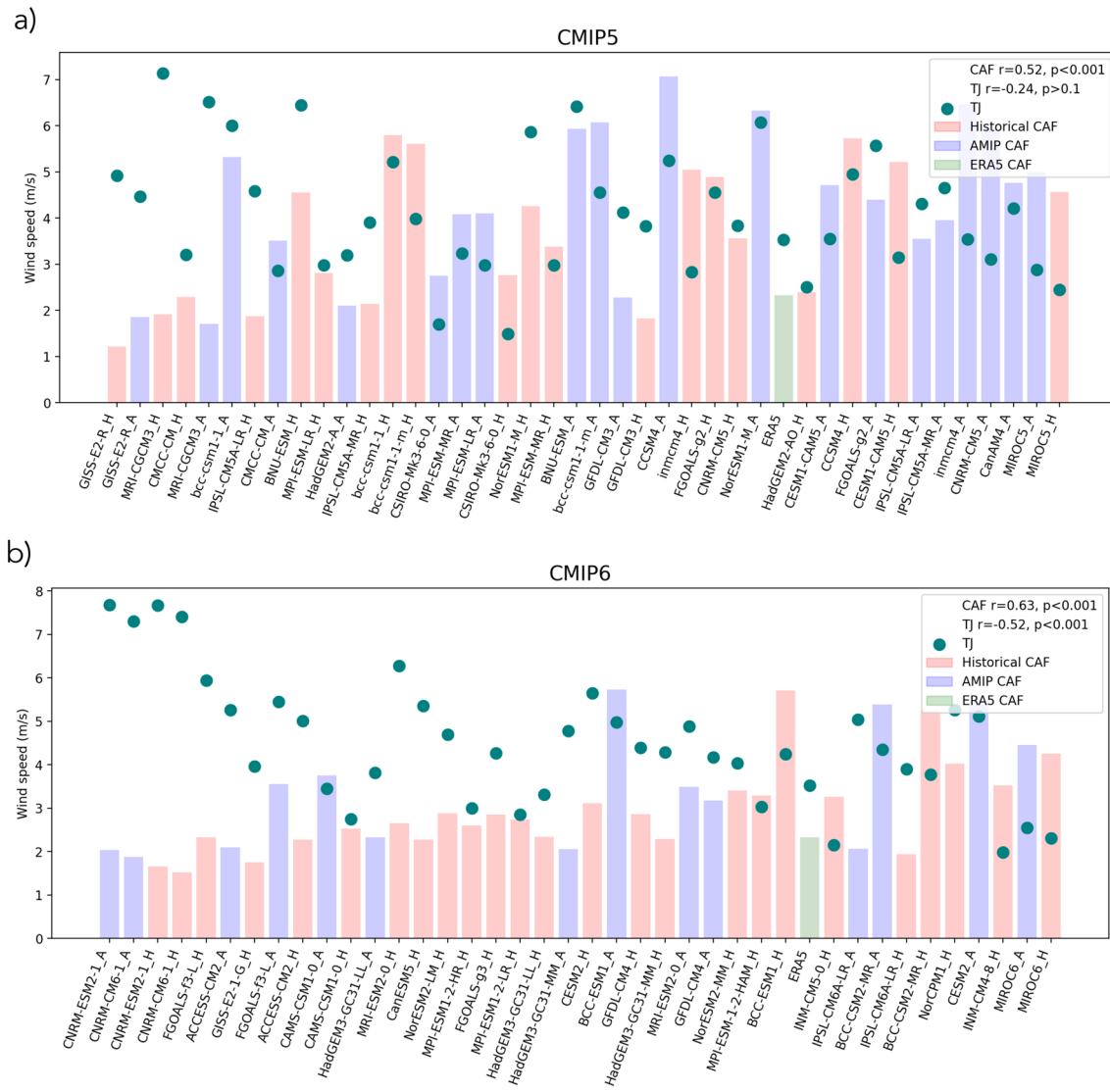


Fig. 15 CMIP5 (a) and CMIP6 (b) TJ and CAF wind speed with models are ordered from driest to wettest along the x-axis. Bars represent baseline mean CAF wind speed. Blue bars represent AMIP

model simulations and red bars represent coupled Historical simulations. The single green bar represents ERA5. Teal dots are the mean TJ strength in the model baseline (1981–2005)

sphere due to zonal mean or Hadley overturning in AMIP simulations, and the strength of warm biases in the southern oceans in coupled Historical simulations.

4. In CMIP6, AH biases in AMIP simulations can be understood using both Hadley, and Walker overturning components. This is not the case in MH biases. SO SST biases persist in CMIP6, but there is a better correlation between MH circulation and warm biases in the WIO.
5. Mean CAF is correlated with GHA masked rainfall in both ensembles, but this is stronger in CMIP6. In CMIP6 mean TJ wind speeds are negatively correlated with GHA masked rainfall indicating potential improvements in the representation of this feature in CMIP6.

We have suggested mechanisms for why AH, MH and therefore the AH-MH metric may be biased in models although further work is required to understand model biases in CMIP6. Such a process-based analysis provides useful framing for impact assessments, informing our confidence in future change. Rather than using this information to select specific models, this adds information to studies on precipitation and rainfall performance (Dyer et al. 2020; Jury 2015). For instance, CMIP5 models that perform well in Dyer et al. (2020) (MPI-ESM-MR, HadGEM-AO, and GFDL-CM3) represent the AH, MH and mixed metric reasonably well even in their coupled simulations.

Based on the results presented here, it will be important to understand the influence of future MH and AH changes on GHA masked rainfall in CMIP6. While some metrics show the MH strengthened in the historical period, He et al. (2017) used a CMIP5 multi-model mean to show that subtropical anticyclones in the south Indian and Atlantic oceans will become weaker with global warming. However, Reboita et al. (2019) show (using HadGEM, GFDL, and MPI in CMIP5) that the AH will expand poleward but shows little change in intensity in an end of century time slice. Investigating the importance of biases in the western Indian Ocean SSTs would be a logical next step as IOD seasonality in CMIP6 has shifted to start earlier in September, with IOD events that are overly strong with increased variability in July and August (McKenna et al. 2020). Connected to the influence of SSTs, biases in the Indian Monsoon (Choudhury et al. 2021) and Walker circulation (Richter and Tokinaga 2020) in CMIP ensembles and their influence on GHA rainfall and subtropical anticyclones will be important to understand as both local and remote drivers of change and variability.

In summary, we have investigated the influence of MH and AH circulation on GHA rainfall during the JAS season and found that increased MH circulation is associated with decreased GHA masked rainfall, with the opposite being so for AH circulation. We have also shown that a mixed metric of AH-MH circulation strength is a better metric for understanding rainfall variability. This metric also relates well to the variability of local circulation features, the TJ and CAF, that influence GHA rainfall. In a process-based assessment we have identified possible causes of biases in the CMIP5 and CMIP6 ensemble representations of the AH and MH, including characteristics of the large-scale overturning in AMIP, and SST biases in the Indian and southern oceans in coupled models. These results will enable better interrogation of the causal relationship between future changes in GHA rainfall and the AH and MH circulation systems in the Indian and Atlantic Oceans.

Supplementary Information The online version contains supplementary material available at <https://doi.org/10.1007/s00382-022-06287-0>.

Author contributions This study was conceptualised by ED and LH. Analysis carried out by ED, developed and interpreted by ED, LH and MT. The write-up of this manuscript was led by ED with LH and MT reviewing and approving this version for submission.

Funding This document is an output from the REACH programme funded by UK Aid from the UK Foreign, Commonwealth and Development Office (FCDO) for the benefit of developing countries (Programme Code 201880). However, the views expressed and information contained in it are not necessarily those of or endorsed by FCDO, which can accept no responsibility for such views or information or for any reliance placed on them. Linda Hirons was also supported by the National Centre of Atmospheric Science (NCAS) ACREW

(Atmospheric hazard in developing Countries: Risk assessment and Early Warning).

Data availability CHIRPSv2 rainfall observations are accessible at (<https://www.chc.ucsb.edu/data/chirps>). TAMSAT rainfall observations are accessible at (<http://www.tamsat.org.uk>). ERA5 reanalysis monthly averaged data on pressure levels can be accessed via the Copernicus Climate Change Service (C3S) (<https://cds.climate.copernicus.eu>). CMIP5 and CMIP6 simulations are available from the Earth System Grid Federation (ESGF) portal at the Centre for Environmental Data Analysis (CEDA) (<https://esgf-index1.ceda.ac.uk/projects/esgf-ceda/>). HadISST SSTs can be downloaded from (<https://www.metoffice.gov.uk/hadobs/hadisst/>).

Declarations

Conflict of interest The authors declare that they have no known competing financial interests or personal relationships that could have appeared to influence the work reported in this paper.

Open Access This article is licensed under a Creative Commons Attribution 4.0 International License, which permits use, sharing, adaptation, distribution and reproduction in any medium or format, as long as you give appropriate credit to the original author(s) and the source, provide a link to the Creative Commons licence, and indicate if changes were made. The images or other third party material in this article are included in the article's Creative Commons licence, unless indicated otherwise in a credit line to the material. If material is not included in the article's Creative Commons licence and your intended use is not permitted by statutory regulation or exceeds the permitted use, you will need to obtain permission directly from the copyright holder. To view a copy of this licence, visit <http://creativecommons.org/licenses/by/4.0/>.

References

- African-SWIFT (2020) Kenyan Lakes reach record levels. GCRF. Retrieved from <https://africanswift.org/2020/09/16/kenyan-lakes-reach-record-levels/>
- Boos WR, Emanuel KA (2009) Annual intensification of the Somali jet in a quasi equilibrium framework: observational composites. *Q J R Meteorol Soc* 135(639):319–335. <https://doi.org/10.1002/qj.388>
- Boschat G, Simmonds I, Purich A, Cowan T, Pezza AB (2016) On the use of composite analyses to form physical hypotheses: an example from heat wave-SST associations. *Sci Rep* 6(1):29599. <https://doi.org/10.1038/srep29599>
- Cabos W, Sein DV, Pinto JG, Fink AH, Koldunov NV, Alvarez F, Jacob D (2017) The South Atlantic Anticyclone as a key player for the representation of the tropical Atlantic climate in coupled climate models. *Clim Dyn* 48(11–12):4051–4069. <https://doi.org/10.1007/s00382-016-3319-9>
- Camberlin P (1995) June–September rainfall in north-eastern Africa and atmospheric signals over the tropics: a zonal perspective. *Int J Climatol* 15(7):773–783. <https://doi.org/10.1002/joc.3370150705>
- Camberlin P (1996) Intraseasonal variations of June–September rainfall and upper-air circulation over Kenya. *Theor Appl Climatol* 54(3–4):107–115. <https://doi.org/10.1007/BF00865153>
- Camberlin P (1997) Rainfall anomalies in the source region of the Nile and their connection with the Indian summer monsoon. *J Clim* 10(6):1380–1392. [https://doi.org/10.1175/1520-0442\(1997\)010h380:RAITSRi2.0.CO;2](https://doi.org/10.1175/1520-0442(1997)010h380:RAITSRi2.0.CO;2)

- Camberlin P, Janicot S, Poccard I (2001) Seasonality and atmospheric dynamics of the teleconnection between African rainfall and tropical sea-surface temperature: Atlantic vs. ENSO. *Int J Climatol* 21(8):973–1005. <https://doi.org/10.1002/joc.673>
- Choudhury BA, Rajesh PV, Zahan Y, Goswami BN (2021) Evolution of the Indian summer monsoon rainfall simulations from CMIP3 to CMIP6 models. *Clim Dyn* 1:1–26. <https://doi.org/10.1007/s00382-021-06023-0>
- Creese A, Washington R (2018) A process-based assessment of CMIP5 rainfall in the Congo basin: the September–November rainy season. *J Clim* 31(18):7417–7439. <https://doi.org/10.1175/JCLI-D-17-0818.1>
- Crossett CC, Metz ND (2017) A climatological study of extreme cold surges along the African highlands. *J Appl Meteorol Climatol* 56(6):1731–1738. <https://doi.org/10.1175/JAMC-D-15-0191.1>
- Davies TD, Vincent CE, Beresford AK (1985) July–August rainfall in West-Central Kenya. *J Climatol* 5(1):17–33. <https://doi.org/10.1002/joc.3370050103>
- Dawson A (2016) Windspharm: a high-level library for global wind field computations using spherical harmonics. *J Open Res Softw.* <https://doi.org/10.5334/jors.129>
- Degefu MA, Rowell DP, Bewket W (2017) Teleconnections between Ethiopian rainfall variability and global SSTs: observations and methods for model evaluation. *Meteorol Atmos Phys* 129(2):173–186. <https://doi.org/10.1007/s00703-016-0466-9>
- Dinku T, Funk C, Peterson P, Maidment R, Tadesse T, Gadain H, Cecatto P (2018) Validation of the CHIRPS satellite rainfall estimates over eastern Africa. *Q J R Meteorol Soc.* <https://doi.org/10.1002/qj.3244>
- Diro GT, Grimes DIF, Black E (2011) Teleconnections between Ethiopian summer rainfall and sea surface temperature: Part I—observation and modelling. *Clim Dyn* 37(1):103–119. <https://doi.org/10.1007/s00382-010-0837-8>
- Dyer E, Washington R, Teferi Taye M (2020) Evaluating the CMIP5 ensemble in Ethiopia: creating a reduced ensemble for rainfall and temperature in Northwest Ethiopia and the Awash basin. *Int J Climatol* 40(6):2964–2985. <https://doi.org/10.1002/joc.6377>
- Exarchou E, Prodhomme C, Brodeau L, Guemas V, Doblas-Reyes F (2018) Origin of the warm eastern tropical Atlantic SST bias in a climate model. *Clim Dyn* 51(5–6):1819–1840. <https://doi.org/10.1007/s00382-017-3984-3>
- Eyring V, Bony S, Meehl GA, Senior CA, Stevens B, Stouffer RJ, Taylor KE (2016) Overview of the Coupled Model Intercomparison Project Phase 6 (CMIP6) experimental design and organization. *Geosci Model Dev* 9(5):1937–1958. <https://doi.org/10.5194/gmd-9-1937-2016>
- Feba F, Ashok K, Ravichandran M (2019) Role of changed Indo-Pacific atmospheric circulation in the recent disconnect between the Indian summer monsoon and ENSO. *Clim Dyn* 52(3–4):1461–1470. <https://doi.org/10.1007/s00382-018-4207-2>
- Fischer AS, Terray P, Guilyardi E, Gualdi S, Delecluse P (2005) Two independent triggers for the Indian Ocean dipole/zonal mode in a coupled GCM. *J Clim* 18(17):3428–3449. <https://doi.org/10.1175/JCLI3478.1>
- Funk C, Peterson P, Landsfeld M, Pedreros D, Verdin J, Shukla S, Michaelsen J (2015) The climate hazards infrared precipitation with stations—a new environmental record for monitoring extremes. *Sci Data* 2(150066):66. <https://doi.org/10.1038/sdata.2015>
- Gleixner S, Keenlyside N, Viste E, Korecha D (2017) The El Niño effect on Ethiopian summer rainfall. *Clim Dyn* 49(5–6):1865–1883. <https://doi.org/10.1007/s00382-016-3421-z>
- He C, Wu B, Zou L, Zhou T (2017) Responses of the summertime subtropical anticyclones to global warming. *J Clim* 30(16):6465–6479. <https://doi.org/10.1175/JCLI-D-16-0529.1>
- Hersbach H, Bell B, Berrisford P, Hirahara S, Horányi A, Muñoz-Sabater J, Thépaut J (2020) The ERA5 global reanalysis. *Q J R Meteorol Soc* 146(730):1999–2049. <https://doi.org/10.1002/qj.3803>
- Hersbach H, Bell B, Berrisford P, Biavati G, Horányi A, Muñoz Sabater J, Thépaut J.-N. (2019). ERA5 monthly averaged data on pressure levels from 1979 to present Copernicus Climate Change Service (C3S) Climate Data Store (CDS). <https://doi.org/10.24381/cds.6860a573>
- Hirons L, Turner A (2018) The impact of Indian Ocean mean-state biases in climate models on the representation of the East African short rains. *J Clim* 31(16):6611–6631. <https://doi.org/10.1175/JCLI-D-17-0804.1>
- Holton JR, Hakim GJ (2012) An introduction to dynamic meteorology: 5th edn, vol 9780123848. Elsevier. <https://doi.org/10.1016/C2009-0-63394-8>
- Hyder P, Edwards JM, Allan RP, Hewitt HT, Bracegirdle TJ, Gregory JM et al (2018) Critical Southern Ocean climate model biases traced to atmospheric model cloud errors. *Nat Commun.* <https://doi.org/10.1038/s41467-018-05634-2>
- James R, Washington R, Abiodun B, Kay G, Mutemi J, Pokam W, Senior C (2018) Evaluating climate models with an African lens. *Bull Am Meteorol Soc* 99(2):313–336. <https://doi.org/10.1175/BAMS-D-16-0090.1>
- Jury MR (2015) Statistical evaluation of CMIP5 climate change model simulations for the Ethiopian highlands. *Int J Climatol* 35(1):37–44. <https://doi.org/10.1002/joc.3960>
- Korecha D, Barnston AG (2007) Predictability of June–September Rainfall in Ethiopia. *Mon Weather Rev* 135(2):628–650. <https://doi.org/10.1175/MWR3304.1>
- Korecha D, Sorteberg A (2013) Validation of operational seasonal rainfall fore cast in Ethiopia. *Water Resour Res* 49(11):7681–7697. <https://doi.org/10.1002/2013WR013760>
- Lee SK, Mechoso CR, Wang C, Neelin JD (2013) Interhemispheric influence of the northern summer monsoons on southern subtropical anticyclones. *J Clim* 26(24):10193–10204. <https://doi.org/10.1175/JCLI-D-13-00106.1>
- Maidment RI, Grimes D, Allan RP, Tarnavsky E, Marcstringer M, Hewison T, Black E (2014) The 30 year TAMSAT African rainfall climatology and time series (TARCAT) data set. *J Geophys Res* 119(18):10619–10644. <https://doi.org/10.1002/2014JD021927>
- Maidment RI, Grimes D, Black E, Tarnavsky E, Young M, Greatrex H et al (2017) A new, long-term daily satellite-based rainfall dataset for operational monitoring in Africa. *Sci Data* 4(1):1–19. <https://doi.org/10.1038/sdata.2017.63>
- Manatsa D, Morioka Y, Behera SK, Matarira CH, Yamagata T (2014) Impact of mazcarne high variability on the East African ‘short rains’. *Clim Dyn* 42(5–6):1259–1274. <https://doi.org/10.1007/s00382-013-1848-z>
- McKenna S, Santoso A, Gupta AS, Taschetto AS, Cai W (2020) Indian Ocean Dipole in CMIP5 and CMIP6: characteristics, biases, and links to ENSO. *Sci Rep* 10(1):1–13. <https://doi.org/10.1038/s41598-020-68268-9>
- Nicholson SE (2014) The predictability of rainfall over the greater horn of Africa. Part I: prediction of seasonal rainfall. *J Hydrometeorol* 15(3):1011–1027. <https://doi.org/10.1175/JHM-D-13-062.1>
- Ogwang BA, Ongoma V, Xing L, Ogou FK (2015) Influence of mazcarne high and Indian Ocean dipole on East African extreme weather events. *Geographica Pannonica* 19(2):64–72. <https://doi.org/10.5937/geopan1502064o>
- Philip S, Kew SF, van Oldenborgh GJ, Otto F, O’Keefe S, Haustein K, Cullen H (2018) Attribution analysis of the Ethiopian drought of 2015. *J Clim* 31(6):2465–2486. <https://doi.org/10.1175/JCLI-D-17-0274.1>
- Randel WJ, Park M (2006) Deep convective influence on the Asian summer monsoon anticyclone and associated tracer variability

- observed with Atmospheric Infrared Sounder (AIRS). *J Geophys Res Atmos* 111(12):D12314. <https://doi.org/10.1029/2005JD006490>
- Rayner NA (2003) Global analyses of sea surface temperature, sea ice, and night marine air temperature since the late nineteenth century. *J Geophys Res* 108(D14):4407. <https://doi.org/10.1029/2002JD002670>
- REACH (2020) Extreme rainfall and management of the Turkwel Gorge Dam in Kenya. Retrieved from <https://reachwater.org.uk/extreme-rainfall-and-the-overflowing-turkwel-gorge-dam-in-kenya/>
- Reboita MS, Ambrizzi T, Silva BA, Pinheiro RF, da Rocha RP (2019) The South Atlantic subtropical anticyclone: present and future climate. *Front Earth Sci* 7(8):1–15. <https://doi.org/10.3389/feart.2019.00008>
- Richter I, Tokinaga H (2020) An overview of the performance of CMIP6 models in the tropical Atlantic: mean state, variability, and remote impacts. *Clim Dyn* 55(9–10):2579–2601. <https://doi.org/10.1007/s00382-020-05409-w>
- Richter I, Mechoso CR, Robertson AW (2008) What determines the position and intensity of the South Atlantic anticyclone in austral winter?—An AGCM study. *J Clim* 21(2):214–229. <https://doi.org/10.1175/2007JCLI1802.1>
- Riddle EE, Cook KH (2008) Abrupt rainfall transitions over the Greater Horn of Africa: observations and regional model simulations. *J Geophys Res Atmos* 113(15):15109. <https://doi.org/10.1029/2007JD009202>
- Rodwell MJ, Hoskins BJ (1996) Monsoons and the dynamics of deserts. *Q J R Meteorol Soc* 122(534):1385–1404. <https://doi.org/10.1256/smsqj.53407>
- Rodwell MJ, Hoskins BJ (2001) Subtropical anticyclones and summer monsoons. *J Clim* 14(15):3192–3211. [https://doi.org/10.1175/1520-0442\(2001\)014h3192:SAASMi2.0.CO;2](https://doi.org/10.1175/1520-0442(2001)014h3192:SAASMi2.0.CO;2)
- Rowell DP (2019) An observational constraint on CMIP5 projections of the East African long rains and Southern Indian Ocean warming. *Geophys Res Lett* 46(11):6050–6058. <https://doi.org/10.1029/2019GL082847>
- Segele ZT, Lamb PJ, Leslie LM (2009a) Large-scale atmospheric circulation and global sea surface temperature associations with horn of Africa June–September rainfall. *Int J Climatol* 29(8):1075–1100. <https://doi.org/10.1002/joc.1751>
- Segele ZT, Lamb PJ, Leslie LM (2009b) Seasonal-to-interannual variability of Ethiopia/Horn of Africa Monsoon. Part I: associations of wavelet-filtered large-scale atmospheric circulation and global sea surface temperature. *J Clim* 22(12):3396–3421. <https://doi.org/10.1175/2008jcli2859.1>
- Segele Z, Leslie L, Tarhule A (2015) Sensitivity of horn of Africa rainfall to regional sea surface temperature forcing. *Climate* 3(2):365–390. <https://doi.org/10.3390/cli3020365>
- Sun L, Semazzi FHM, Giorgi F, Ogallo L (1999) Application of the NCAR Regional Climate Model to eastern Africa: 2. Simulation of interannual variability of short rains. *J Geophys Res: Atmos* 104(D6):6549–6562. <https://doi.org/10.1029/1998JD200050>
- Tanaka H, Ishizaki N, Kitoh A (2004) Trend and interannual variability of Walker, monsoon and Hadley circulations defined by velocity potential in the upper troposphere. *Tellus A: Dyn Meteorol Oceanogr* 56(3):250–269. <https://doi.org/10.3402/tellusa.v56i3.14410>
- Tarnavsky E, Grimes D, Maidment R, Black E, Allan RP, Stringer M, Kayitakire F (2014) Extension of the TAMSAT satellite-based rainfall monitoring over Africa and from 1983 to present. *J Appl Meteorol Climatol* 53(12):2805–2822. <https://doi.org/10.1175/JAMC-D-14-0016.1>
- Taye MT, Dyer E, Charles KJ, Hirons LC (2021) Potential predictability of the Ethiopian summer rains: understanding local variations and their implications for water management decisions. *Sci Total Environ* 755:142604. <https://doi.org/10.1016/j.scitotenv.2020.142604>
- Taylor KE, Stouffer RJ, Meehl GA (2012) An overview of CMIP5 and the experiment design. *Bull Am Meteorol Soc* 93(4):485–498. <https://doi.org/10.1175/BAMS-D-11-00094.1>
- Terray P, Delecluse P, Labattu S, Terray L (2003) Sea surface temperature associations with the late Indian summer monsoon. *Clim Dyn* 21(7–8):593–618. <https://doi.org/10.1007/s00382-003-0354-0>
- Terray P, Dominik S, Delecluse P (2005) Role of the southern Indian Ocean in the transitions of the monsoon-ENSO system during recent decades. *Clim Dyn* 24(2–3):169–195. <https://doi.org/10.1007/s00382-004-0480-3>
- Vidya P, Ravichandran M, Subeesh MP, Chatterjee S, Nuncio M (2020) Global warming hiatus contributed weakening of the Mascarene High in the Southern Indian Ocean. *Sci Reports* 10(1):1–9. <https://doi.org/10.1038/s41598-020-59964-7>
- Viste E, Sorteberg A (2013) Moisture transport into the Ethiopian highlands. *Int J Climatol* 33(1):249–263. <https://doi.org/10.1002/joc.3409>
- Viste E, Korecha D, Sorteberg A (2013) Recent drought and precipitation tendencies in Ethiopia. *Theor Appl Climatol* 112(3–4):535–551. <https://doi.org/10.1007/s00704-012-0746-3>
- Vizy EK, Cook KH (2003) Connections between the summer east African and Indian rainfall regimes. *J Geophys Res: Atmos* 108(16):4510. <https://doi.org/10.1029/2003jd003452>
- Vizy EK, Cook KH (2019) Observed relationship between the Turkana low-level jet and boreal summer convection. *Clim Dyn* 53(7–8):4037–4058. <https://doi.org/10.1007/s00382-019-04769-2>
- Vizy EK, Cook KH (2020) Interannual variability of East African rainfall: role of seasonal transitions of the low-level cross-equatorial flow. *Clim Dyn* 54(11–12):4563–4587. <https://doi.org/10.1007/s00382-020-05244-z>
- Wang C, Zhang L, Lee S (2014) A global perspective on CMIP5 climate model biases. *Nat Clim Change* 4(February):201–205. <https://doi.org/10.1038/NCLIMATE2118>
- Williams AP, Funk C, Michaelsen J, Rauscher SA, Robertson I, Wils TH, Loader NJ (2012) Recent summer precipitation trends in the Greater Horn of Africa and the emerging role of Indian Ocean sea surface temperature. *Clim Dyn* 39(9–10):2307–2328. <https://doi.org/10.1007/s00382-011-1222-y>
- Zeleke T, Giorgi F, Mengistu Tsidu G, Diro GT (2013) Spatial and temporal variability of summer rainfall over Ethiopia from observations and a regional climate model experiment. *Theor Appl Climatol* 111(3–4):665–681. <https://doi.org/10.1007/s00704-012-0700-4>

Publisher's Note Springer Nature remains neutral with regard to jurisdictional claims in published maps and institutional affiliations.